




RESEARCH ARTICLE

Genetic mouse models of autism spectrum disorder present subtle heterogenous cardiac abnormalities

Stephania Assimopoulos^{1,2,3}  | Christopher Hammill^{1,2}  | Darren J. Fernandes^{1,2} | Tara Leigh Spencer Noakes^{1,2} | Yu-Qing Zhou¹ | Lauryl M. J. Nutter^{2,4}  | Jacob Ellegood^{1,2} | Evdokia Anagnostou⁵ | John G. Sled^{1,2,3} | Jason P. Lerch^{1,2,3,6}

¹Mouse Imaging Centre, Hospital for Sick Children, Toronto, Ontario, Canada

²Sickkids Research Institute, The Hospital for Sick Children, Toronto, Ontario, Canada

³Department of Medical Biophysics, University of Toronto, Toronto, Ontario, Canada

⁴The Centre for Phenogenomics, Toronto, Ontario, Canada

⁵Bloorview Research Institute, Holland Bloorview Kids Rehabilitation Hospital, Toronto, Ontario, Canada

⁶Wellcome Centre for Integrative Neuroimaging, The University of Oxford, Oxford, UK

Correspondence

Stephania Assimopoulos, Mouse Imaging Centre, Hospital for Sick Children, Toronto, Ontario, Canada.

Email: stephania.assimopoulos@sickkids.ca

Funding information

Canadian Institutes of Health Research; Hospital for Sick Children

Abstract

Autism spectrum disorder (ASD) and congenital heart disease (CHD) are linked on a functional and genetic level. Most work has investigated CHD-related neurodevelopmental abnormalities. Cardiac abnormalities in ASD have been less studied. We investigated the prevalence of cardiac comorbidities relative to ASD genetic contributors. Using high frequency ultrasound imaging, we screened 9 ASD-related genetic mouse models (*Arid1b*^{+/-}, *Chd8*^{+/-}, 16p11.2 (deletion), *Sgsh*^{+/-}, *Sgsh*^{-/-}, *Shank3 Δexon 4-9*^{+/-}, *Shank3 Δexon 4-9*^{-/-}, *Fmr1*^{-/-}, *Vps13b*^{+/-}), and pooled wild-type littermates (WTs). We measured heart rate (HR), aorta diameter (AoD), thickness and thickening of the left-ventricular (LV) anterior and posterior walls, LV chamber diameter, fractional shortening, stroke volume and cardiac output, mitral inflow Peak E and A velocity ratio, ascending aorta velocity time integral (VTI). Mutant groups presented small-scale alterations in cardiac structure and function compared to WT (LV anterior wall thickness and thickening, chamber diameter and fractional shortening, HR). A greater number of significant differences was observed among mutant groups than between mutant groups and WT. Mutant groups differed primarily in structural measures (LV chamber diameter and anterior wall thickness, HR, AoD). The mutant groups with most differences to WT were 16p11.2 (deletion), *Fmr1*^{-/-}, *Arid1b*^{+/-}. The mutant groups with most differences from other mutant groups were 16p11.2 (deletion), *Sgsh*^{+/-}, *Fmr1*^{-/-}. Our results recapitulate the associated clinical findings. The characteristic ASD heterogeneity was recapitulated in the cardiac phenotype. The type of abnormal measures (morphological, functional) can highlight common underlying mechanisms. Clinically, knowledge of cardiac abnormalities in ASD can be essential as even non-lethal abnormalities impact normal development.

Lay Summary

Autism spectrum disorder (ASD) and congenital heart disease (CHD) are linked functionally and genetically. ASD cardiac phenotyping is limited. We assessed the cardiac phenotype of 9 ASD-related mouse models. We found subtle heterogeneous cardiac abnormalities compared to controls, with more differences within ASD than between ASD and controls, mirroring clinical findings. Clinically, knowing the cardiac abnormalities in ASD is vital as even non-lethal cardiac abnormalities can impact development.

KEYWORDS

autism, cardiac phenotype/cardiology, comorbidities, genetic mouse models, phenotyping, ultrasound biomicroscopy

This is an open access article under the terms of the [Creative Commons Attribution-NonCommercial-NoDerivs](https://creativecommons.org/licenses/by-nc-nd/4.0/) License, which permits use and distribution in any medium, provided the original work is properly cited, the use is non-commercial and no modifications or adaptations are made.

© 2022 The Authors. *Autism Research* published by International Society for Autism Research and Wiley Periodicals LLC.

INTRODUCTION

Autism spectrum disorder (ASD) and congenital heart disease (CHD) have been found to be strongly linked both on a functional (Kaltman et al., 2005; Limperopoulos et al., 2010; Sun et al., 2015) and a genetic level (Homsy et al., 2015; Pierpont et al., 2018; Tsao et al., 2017). ASD is a neurodevelopmental disorder (NDD) with an occurrence rate >1%, highly heterogeneous in etiology and phenotype (Amaral, 2011; Amaral et al., 2011). It is primarily associated with behavioral deficits, but also has associated comorbidities, amongst which cardiac are common (Tyler et al., 2011). These cardiac comorbidities can be congenital or not.

The association between neurodevelopmental and cardiac abnormalities has been primarily studied in the context of congenital heart disease (CHD). Specifically, great focus has been put into identifying the frequency of neurodevelopmental differences in various CHD cases.

CHD is the most common birth defect (0.8%–1.2% of all live births; Hoffman & Kaplan, 2002; Wu et al., 2020), accounting for ~3% of infant deaths, 46% of which are due to congenital malformations (Sadowski, 2009). Neurodevelopmental differences, including language, motor, cognitive and social deficits, occur in 10% of children with congenital heart disease and in 50% of those with severe congenital heart disease (Marino et al., 2012). Brain development is found to be atypical on MRI studies, with newborns having smaller for gestational age total brain volume, reduced metabolism, and delayed cortical development and folding compared to controls (following age and weight adjustment; Clouchoux et al., 2012; Licht et al., 2009; Limperopoulos et al., 2010; Miller et al., 2007; Ortinau et al., 2018), both prior to and following the necessary corrective cardiac surgeries (Limperopoulos et al., 2010; Ortinau et al., 2018). Moreover, known risk factors can only account for 30% of the neurodevelopmental outcome following such interventions, suggesting there are other genetic and epigenetic factors contributing to the outcomes (Gaynor et al., 2007). There are only a few studies on specifically the ASD-CHD association, and they report an increased risk of ASD in CHD (Sigmon et al., 2019; Tsao et al., 2017).

Cardiac and neurodevelopmental abnormalities have also been jointly studied in terms of their genetic underpinnings with the goal of identifying underlying genetic similarities. A large study performing exome sequencing on 1213 congenital heart disease parent-offspring trios identified 69 genes containing damaging de novo mutations known to be associated with both ASD and NDD, all of which are in the top quartile of both developmental heart and brain expression (far more than expected by chance), thus revealing a shared genetic contribution to CHD and NDD (Homsy et al., 2015). Furthermore, recent studies using network genetics analysis identified a convergent molecular network underlying ASD and

CHD pinpointing 101 genes with shared genetic risk for both (Rosenthal et al., 2021). as well as a shared network underlying ASD and cardiomyopathy (Nazeen et al., 2016). Other studies have identified ASD-related genes with a prevalence of cardiac abnormalities (both congenital and not; *FMRI*, *ARID1B*, *ANK2*, *CHD2*, *CHD7* etc.; de Rubeis & Buxbaum, 2015; Pierpont et al., 2018), as well as loci with a pleiotropic function between the heart and the brain (16p11.2 [deletion], 22q11.2, 10q24; Pierpont et al., 2018; Webb, Erdmann, et al., 2017).

Contrary to the aforementioned work on NDDs in CHD, the investigation of cardiac abnormalities in ASD, whether specifically CHD or not, has been more limited. The incidence rate of cardiac abnormalities reported in ASD varies in the literature depending on the cardiac abnormalities considered and the age of the subjects. In an adult U.S.A. population sample, Croen et al. (2015) considered three categories of cardiovascular diseases (dyslipidemia, hypertension and all other) and reported a joint prevalence of 36.96% and an odds ratio of 2.54, with hypertension being the most prevalent amongst the three groups (Croen et al., 2015). Similarly, in an adult French population subset, Miot et al. (2019) considered five categories of which three were significant (heart failure, orthostatic hypotension, peripheral vascular disease) and reported a joint prevalence of 15.37%, while separately considering hypertension with a prevalence of 13.56% (Miot et al., 2019). A population study in Western Australia assessing the occurrence rate of birth defects diagnosed before the age of 6 in children with ASD, reported a 1.3% incidence rate with a 1.2 odds ratio for cardiovascular system defects (Dawson et al., 2009).

Considering all reports on ASD cardiac phenotype in literature, we see that ASD is associated with a vast spectrum of cardiac abnormalities. Overarching patterns include morphological alterations and cardiac dysrhythmias (ventricular flutter, fibrillation, and premature beats). These abnormalities are present in both ASD and ASD-related NDDs.

In non-syndromic (idiopathic) ASD reduced resting-state heart rate (HR) variability, slowed respiratory sinus arrhythmia (RSA) and/or increased HR have been reported (Benevides & Lane, 2013; Bujnakova et al., 2016; Sheinkopf et al., 2019). In syndromic ASD both functional and morphological abnormalities have been reported. Examples of syndromic ASD presenting cardiac abnormalities are Coffin-Siris syndrome (*ARID1B* mutation), Timothy syndrome (*CACNA1C* mutation), Rett syndrome (*MECP2* mutation) and Fragile X syndrome (*FMRI* mutation). The *ARID1B* gene, besides being a prominent autism-related gene, is also associated with CHD with a prevalence in 20% of CHD cases (Homsy et al., 2015; Pierpont et al., 2018). In *ARID1B* mutation various structural abnormalities have been reported (Homsy et al., 2015; Pierpont et al., 2018;

Tables S1 and S2). In Timothy syndrome, cardiac abnormalities vary depending on the type of pathogenic variant present. In gain-of-abnormal-function pathogenic variants various cardiac arrhythmias, even leading to sudden death, as well as cardiovascular malformations are present (Napolitano et al., 2006). In loss-of-function variants cardiac arrhythmias are widely reported (Boczek et al., 2015; Napolitano et al., 2006). In Rett syndrome (*MECP2* mutation; 95% ASD prevalence) severe cardiac arrhythmias, abnormal ventricular repolarisation and systo-diastolic biventricular myocardial dysfunction are reported (Acampa & Guideri, 2006; de Felice et al., 2012). Finally, morphological cardiac abnormalities have been reported in (and Fragile X syndrome (*FMRI* mutation) including mitral valve anomalies, aortic root dilation, and arrhythmias (Berry-Kravis et al., 2019; Ciaccio et al., 2017; Ornoy et al., 2016; Pierpont et al., 2018; Tassanakijpanich et al., 2020; Tables S1 and S2).

Related investigations have been conducted for other ASD-related NDDs, such as Trisomy21 (Down Syndrome), chromosomal disorders of 22q11 deletion syndrome (DiGeorge, velocardiofacial syndrome) and CHARGE syndrome. Trisomy 21 (Down syndrome; ASD prevalence 5%–39%; Moss & Howlin, 2009; Morales-Demori, 2017) congenital heart disease is present in 50% of patients (Metcalf, 2018). In 22q11 deletion syndromes (ASD prevalence of 15%–50%; Vorstman et al., 2006) cardiac dysrhythmias and various morphological defects are prominent (Doshi-Velez et al., 2014; Lee et al., 2014; Metcalf, 2018). Even more, the co-existence of a cardiac abnormality has been found to also result in reduced cortical and hippocampal volume (Debbané et al., 2014). CHARGE syndrome, a genetic disorder manifested through a non-random association of congenital anomalies (Pagon et al., 1981), with ASD prevalence of 15%–50% (Moss & Howlin, 2009), has a known associated cardiac dysfunction (Blake & Prasad, 2006; Corsten-Janssen et al., 2013; Meisner & Martin, 2020).

Finally, accumulating evidence suggests that severe cardiac abnormalities do not simply co-occur with NDDs but may also contribute to the observed neurodevelopmental abnormalities (Doshi-Velez et al., 2014; Gaynor et al., 2007; Limperopoulos et al., 2010), thus further highlighting the need for deeper investigation of cardiac abnormalities in ASD.

It is apparent that cardiac comorbidities in ASD may arise as a result of various, potentially coinciding, factors. In this work, we investigate the prevalence of cardiac comorbidities relative to prominent genetic contributors of ASD. Specifically, using high frequency ultrasound imaging, we screen a set of ASD-related genetic mouse models with a standardized protocol to assess the incidence of cardiac abnormalities.

This study is performed in mice to allow for tightly controlled genetics, environment and experimental procedures. Studies in mouse models of ASD have been useful in

determining the impact of genomic variation on brain differences across species (Ellegood & Crawley, 2015; Lázaro & Golshani, 2015). For the same reasons, model organisms have been employed in the study of heart development and disease. In the adult heart, overall, only subtle cardiac differences are present between mammalian species. Specifically, in the case of the mouse, the ventricular and valvular structures are the same while any structural differences that exist mainly involve atrial and venous parts (Doevendans et al., 1998; Krishnan et al., 2014). Cardiac excitation, contraction, and relaxation are also found to be comparable between adult mouse and human (Milani-Nejad & Janssen, 2014; Wessels & Sedmera, 2004). Finally, various mouse models of CHD have been reported to adequately replicate the corresponding human condition suggesting that mouse models may be well suited for this endeavor (Snider & Conway, 2011).

However, it can be useful when interpreting our results to note certain functional differences that exist between the human and mouse heart. The mouse has a significantly higher heart rate than humans, and, by extension, the mouse heart has a higher metabolic and contraction rate (Hamlin & Altschuld, 2011; Janssen et al., 2016; Milani-Nejad & Janssen, 2014). In the mouse, the sinoatrial (SA) node (the heart's "pace-maker") is found outside the right atrium (RA), while in humans it is inside (Chandler et al., 2011; Doevendans et al., 1998; Wen & Li, 2015). However, the innervation of the heart, from the atrioventricular (AV) node to the bundle of His branches, is conserved from smaller to larger animals (Doevendans et al., 1998; Henk Van Der Tweel et al., 1999; Noujaim et al., 2004). Stroke volume and heart index are comparable between mice and humans after correcting for body surface (Doevendans et al., 1998; Patel & Makaryus, 2020; Pet et al., 2006). However, a difference exists in the percent of cardiac output reaching the brain; 3% for mice and ~12% for humans (Doevendans et al., 1998; Milani-Nejad & Janssen, 2014). This difference can be reflective of the relative weights of the tissues in each species (Doevendans et al., 1998). Finally, another functional difference involves the role of RV relaxation to ventricular filling. In mice during diastole ventricular filling is dominated by the LV active relaxation, while the RV active relaxation makes less of a contribution. Conversely, in adult humans the contribution is roughly the same for both (Habib & Zoghbi, 1992; Zhou et al., 2004; Zoghbi et al., 1990). The underlying mechanisms driving this difference are still to be explored (Zhou et al., 2004).

METHODS

Animals

Adult (60 days old ± 1 day) male mice from 9 mouse models of 7 ASD-related genes (Table 1) were used in this

TABLE 1 Mouse models used in the study given by their common name and official mouseline name. Genotype and number of mice used per model also listed

Mouse model: Common name	Mouseline	Genotype	Number of mice
Sgsh-Het	C57BL/6NCrl-Sgsh ^{em3(IMPC)Tep} /Cmmr	(+/-)	20
Sgsh-Hom	C57BL/6NCrl-Sgsh ^{em3(IMPC)Tep} /Cmmr	(-/-)	20
Fmr1	B6:129P2-Fmr1/n	(-Y)	20
Arid1b	C57BL/6NCrl-Arid1b ^{em1(IMPC)Tep} /Cmmr	(+/-)	20
Shank3-Het (Δ exon 4-9)	B6(Cg)-Shank3 ^{tm1.2Bux} /n	(+/-)	20
Shank3-Hom (Δ exon 4-9)	B6(Cg)-Shank3 ^{tm1.2Bux} /n	(-/-)	20
16p11.2 deletion	B6.129S-Del(7Slx1b-Sept1)4Aam/n	(df/+)	20
Chd8	C57BL/6J-Chd8 ^{em1Tep}	(+/-)	20
Vps13b	C57BL/6NCrl-Vps13b ^{em1(IMPC)Tep} /Cmmr	(+/-)	20
Wild-type (WT)	-	(+/+)	21

study. We chose a range of different genetic models with respect to their relevance to ASD and their documented cardiac phenotype. From single-gene mutation models we chose *ARID1B*, *CHD8*, *FMRI*, *SGSH* and *VPS13B*. We also chose to interrogate two CNV models, 16p11.2 (deletion) and Shank3 (Δ exon 4-9),

ARID1B and *CHD8* are prominent ASD-related genes with strong association to cardiac abnormalities/congenital heart disease. Specifically, *ARID1B* is a cross-linked gene between ASD and congenital heart disease, with approximately 20% prevalence of congenital heart disease (Homsy et al., 2015; Pierpont et al., 2018). Reported abnormalities include mitral valve insufficiency, septal defects, and atrioventricular (AV) block (Pierpont et al., 2018). *ARID1B* loss-of-function mutations have been found to upregulate the Wnt/ β -catenin signaling pathway (Vasileiou et al., 2015). Studies in the mouse have shown β -catenin contributes to the regulation of postnatal hypertrophic growth by acting upstream of fibroblast growth factor (FGF) signaling. FGF signaling regulates second heart field (SHF) progenitors that give rise to the atrial, ventricular and outflow tract structures (Cohen et al., 2008; Hubert et al., 2018).

CHD8 is also involved in the Wnt signaling pathway through the regulation of β -catenin (Cotney et al., 2015). Additionally, in the mouse, Chd8 mRNA has been detected in high levels during early embryogenesis and up to 10 days postnatally with a drop-off in concentration thereafter (Nishiyama et al., 2011). Complete knockout of *CHD8* leads to in utero embryonic demise following severe hemorrhage, indicative of cardiovascular defects (Nishiyama et al., 2011). In the rat, Chd8 has been detected during embryonic and postnatal cardiac development in myocytes and fibroblasts (Shanks et al., 2012). Chd8 has been proposed to be a new AKAP (A-kinase anchoring protein) in humans. Defects in the AKAP function have been shown to lead to arrhythmias, hypertrophy and eventual progression to heart failure (Shanks et al., 2012). Finally, the indirect link of *CHD8* to cardiac dysfunction in CHARGE syndrome may be suggestive of

an involvement in cardiac function (Batsukh et al., 2010). Specifically, CHARGE syndrome, which includes, amongst others, congenital cardiac abnormalities, is characterized by a dysfunction of the *CHD7* gene (Meisner & Martin, 2020). The Chd8 protein is an interacting partner of the Chd7 protein. Changes in interacting proteins necessary for the function of Chd7, such as Chd8, have been proposed as an underlying cause of the disease (Batsukh et al., 2010).

Fragile X syndrome results from a mutation in the *FMRI* gene and is one of the syndromes with high ASD comorbidity (30%; Hagerman et al., 2010). Additionally, cardiac abnormalities have been reported in FMR1 patients, primarily mitral valve prolapse (MVP), aortic root dilation, and arrhythmias (Berry-Kravis et al., 2019; Ciaccio et al., 2017; Ornoy et al., 2016; Pierpont et al., 2018; Tassanakijpanich et al., 2020). An occurrence rate of congenital heart disease <10% has also been reported (Pierpont et al., 2018).

SGSH was chosen as a gene resulting in a progressive disorder (San Filippo syndrome) with an association to ASD albeit not as strong as the previously mentioned genes (Rumsey et al., 2014; Wijburg et al., 2013). In terms of the documented cardiac phenotype, there are reports of cardiomyopathy and progressive valvular disease amongst patients carrying a mutation in the *SGSH* gene (Dangel, 1998; Marques Ribeiro et al., 2014; Nijmeijer et al., 2019).

VPS13B is the only exception as it was chosen as a new mouse model related to ASD that became available to our lab around the time of our study design. Thus, little information existed at the time on associated cardiac abnormalities with mostly normal heart anatomy is reported. Abnormal phenotypes reported most consistently include essential and pulmonary hypertension and cardiac systolic murmurs (Kivitie-Kallio et al., 1999; Kivitie-kallio & Norio, 2001; Rodrigues et al., 2018).

16p11.2 (deletion) and Shank3 (Δ exon 4-9), are both strongly related to ASD and have associated cardiac abnormalities. 16p11.2 microdeletion has been found to

have a pleiotropic function between the heart and the brain (Webb, Erdmann, et al., 2017). Even more, the 16p11.2 locus harbors genes linked to aortic valve development (*BCKDK*, *MAPK3*, *SRCAP*; Ghebranious et al., 2007; Sun & Wang, 2016; Wang, 2007; Xie et al., 2019; Xu et al., 2021). Congenital heart disease has been reported in 33% of patients, specifically, Tetralogy of Fallot (ToF), bicuspid aortic valve and pulmonary atresia (Pierpont et al., 2018). In the case of *Shank3* (*Δexon 4–9*), abundant *Shank3* mRNA has been detected in the heart, while mouse studies have demonstrated the involvement of *Shank3* in myocardial remodeling following myocardial infarction (Cusmano-ozog et al., 2007; Lim et al., 1999; Man et al., 2020). Even more, in Phelan-McDermid syndrome (*Shank3* microdeletion), a series of cardiac abnormalities have been reported in patients, with a prevalence of congenital heart disease >25% (patent ductus arteriosus, ventricular and atrial septal defects, total anomalous pulmonary venous return; Phelan & McDermid, 2012; Pierpont et al., 2018).

A summary table of the above information can be found in the Table S1.

The abnormalities and their effects, resulting from the underlying genetic mutations, can emerge at varying timepoints in development and potentially become more pronounced with time. Thus, by phenotyping our mice at an adult age, we aim to target potentially more stable and more pronounced phenotypes. For the *Arid1b*, *Chd8*, *Vps13b* groups, heterozygous (+/–) mutant mice were assessed, while for the *Fmr1* group, homozygous (–/–) mutant mice were assessed. For the *Sgsh* and *Shank3* (*Δexon 4–9*) groups, we assessed both heterozygous (+/–) and homozygous (–/–) mutant mice. Our control group comprised of 2 wild-type (+/+) littermates from each model (with the exception of *Shank3* where we had 3), pooled across all models. The models for *Arid1b*, *Chd8*, *Vps13b*, and *Sgsh*, were produced at The Centre for Phenogenomics and provided by the Canadian Mutant Mouse Repository (CMMR, Toronto ON). They were all created on a C57BL/6NCr1 background (Charles River Laboratories, strain code 027). The mouse models *Fmr1* (Jackson Laboratory #003025; The Dutch-Belgian Fragile X Consortium et al., 1994), 16p11.2 deletion (Jackson Laboratory #013128; Horev et al., 2011) and *Shank3* (*Δexon 4–9*; Jackson Laboratory #017890; Bozdagi et al., 2010) were obtained from Jackson Laboratory and were backcrossed at least seven generations to C57BL/6NCr1 (Charles River Laboratories, strain code 027). All procedures involving animals were performed in compliance with the Animals for Research Act of Ontario and the Guidelines of the Canadian Council on Animal Care. The Centre for Phenogenomics (TCP) Animal Care Committee reviewed and approved all procedures conducted on animals at TCP.

The number of mice comprising each group is also listed in Table 1 and was determined following a power analysis with significance level $\alpha = 0.05$ and power $\beta = 0.85$.

Animal preparation

Mice were prepared as described by Zhou et al. (2004). They were anesthetized using isoflurane (induced at 5% in medical oxygen, and then maintained at 1.5% through a face mask). Mice were positioned supine with four paws taped to electrodes on a pre-warmed platform for ECG recording and heart rate monitoring. ECG recordings were monitored in real time throughout the scan in order to assure a consistent HR range was maintained. A consistent HR range during one scan and between scans is essential as HR can affect ultrasound measurements. On our ultrasound system, the ECG recordings cannot be saved, so they were not used in our analysis. Mouse body temperature was also monitored by rectal thermometer (Indus Instruments, Houston, TX) and maintained around 36–37°C by a heated platform. Mouse hair on the whole chest was cleanly removed using hair-removal cream (Nair, Carter-Horner, Mississauga, Ontario). Finally, a prewarmed ultrasound gel (Aquasonic 100; Parker Laboratories, Orang, NJ) was used as a coupling medium between the transducer and mouse body for image acquisition.

Imaging

A high frequency ultrasound imaging system (Vevo 2100, FUJIFILM VisualSonics, Inc., Toronto) with a 30 MHz linear array transducer was used for assessing cardiac structure, function and hemodynamics, mainly following an imaging protocol published previously (Foster et al., 2009; Zhou et al., 2004). Unbiased screening of all models was performed using a standardized battery of measures utilizing four conventional function modalities of ultrasound imaging for a full cardiac assessment. Table 2 lists the imaging modalities, approaches/sections and measurements of interest. With the exception of HR, values for all metrics were obtained by averaging the measurements from three cardiac cycles in the same ultrasound recording.

All measures were obtained at least twice in different views/axes/traces (e.g., from the left and right parasternal imaging windows or the short and long axis views of the heart). These measures were treated as duplicates/repeats in the data analysis.

Table 3 lists the cardiac parameters derived from the preliminary ultrasound measurements, and the formula for the related calculations.

Data analysis

Statistical analysis was performed in R3.6.1 (R Core Team, 2019) using the RStudio interface (RStudio, 2019) and the brms (Bürkner, 2017, 2018), loo (Vehtari

TABLE 2 Four ultrasound imaging modalities used for full cardiac assessment, their technical description and the measurements obtained with each

Ultrasound imaging modalities	Technical description	Information and measurements obtained
B-Mode	<ul style="list-style-type: none"> Two-dimensional gray-scale anatomical image Spatial resolution: 100 μm (lateral), 50 μm (axial) Max field-of-view (FOV): 14 mm Max frame rate when image width reduced to minimum: 1000 fps 	<ul style="list-style-type: none"> Overall morphology of the heart Guidance for M-mode and Doppler recordings Distance and area measurements: Diameter of aortic orifice (AoD) during systole - measured from both left and right parasternal imaging windows
M-mode	<ul style="list-style-type: none"> Recording of dynamic changes in position and dimension of the heart or vessel of interest in a chosen direction over a cardiac cycle. Derive dimensional and functional parameters. 	<ul style="list-style-type: none"> Left Ventricle (LV) chamber diameter at end-systole (LV ESD) and end-diastole (LV EDD)—measured in both long and short axis views. Left Ventricle (LV) anterior and posterior wall thickness at end-systole (LV AWes, PWes) and end-diastole (LV AWed, PWed)—measured in both long and short axis view. Heart Rate (HR).
Doppler Color Flow Mapping	<ul style="list-style-type: none"> Visualize blood flow and its direction in different colors. Qualitative demonstration of velocity distribution across heart chamber, orifice or vascular lumen. Proper settings for the pulse repetition frequency (PRF)/velocity scale, gain and threshold of wall filtering. 	<ul style="list-style-type: none"> Guidance for pulse wave Doppler velocity measurement at the sites of interest. Visualize the abnormal flow patterns such high velocity flow jets.
Pulse Wave Doppler	<ul style="list-style-type: none"> Recording of blood flow velocity spectrum at site of interest. Adjustable sample volume size to target vessel size. Angle correction required for accurate measurement. Angle between ultrasound beam and flow less than 60 degrees. 	<ul style="list-style-type: none"> Peak E and A velocity ratio of mitral inflow for left ventricular diastolic function. Velocity Time Integral (VTI) of flow through the vascular lumen such as the ascending aorta or aortic orifice for calculating the flow rate. Heart Rate (HR).

et al., 2020) and bayesplot packages (Gabry et al., 2019; Gabry & Goodrich, 2017; Gelman, 2013; Stan Development Team, 2017).

For each measure, we fit a Bayesian model with partial pooling to the Z-score values of our data, with mouse group and intercept as predictors and a random effect of mouse ID to account for redundancy in certain measures (measured more than once in different axes). We evaluated the need to account for a heteroscedasticity by comparing a model where variance of the posterior distribution varies between mouse groups (Equation 1-A) versus a model with uniform variance across all groups (Equation 1-B). All equations, including the priors used, can be found in Equation (1).

(A) Heteroscedastic model:

$$y_i \sim \mathcal{N}(\mu_{j,k,m_i}, \sigma_{j,k,i}^2)$$

$$\mu_{j,k,m_i} = \beta_{j,k,i}^0 + \beta_{j,k,i}^1 \cdot group_{j,k,i} + \beta_{m_i}$$

$$\sigma_{j,k,m} = \gamma_{j,k}^0 + \gamma_{j,k}^1 \cdot group_{j,k}$$

Intercept prior:

$$\beta_{j,k,i}^0 \sim Student^+(0, 2.5, 3)$$

Group effect prior:

$$\beta_{j,k,i}^1 \sim Unif(-\infty, +\infty)$$

Random effect prior:

$$\beta_{m_i} \sim \mathcal{N}(0, \sigma_{m_i}^2)$$

Random effect standard deviation prior:

$$\sigma_{m_i} \sim Student^+(0, 2.5, 3)$$

Intercept prior of standard deviation σ_{jkm} :

$$\gamma_{j,k}^0 \sim Student^+(0, 2.5, 3)$$

TABLE 3 All the morphological and functional cardiac measures used in the study

Measure	Full name	Class—Acquisition method	Type	Acquisition details
AoD	Diameter of aortic orifice during systole	Measured	Morphological	Measured in both left and right parasternal imaging windows.
VTI	Velocity Time Integral of flow through the ascending aorta.	Measured	Functional	
LVESD	Left Ventricle (LV) chamber diameter at end-systole	Measured	Morphological	Measured in both long and short axis views of the heart.
LVEDD	Left Ventricle (LV) chamber diameter at end-diastole	Measured	Morphological	Measured in both long and short axis views of the heart.
LV AWes	Left Ventricle (LV) anterior wall thickness at end-systole	Measured	Morphological	Measured in both long and short axis views of the heart.
LV AWed	Left Ventricle (LV) anterior wall thickness at end-diastole	Measured	Morphological	Measured in both long and short axis views of the heart.
LV PWes	Left Ventricle (LV) posterior wall thickness at end-systole	Measured	Morphological	Measured in both long and short axis views of the heart.
LV PWed	Left Ventricle (LV) posterior wall thickness at end-diastole	Measured	Morphological	Measured in both long and short axis views of the heart.
HR	Heart rate	Measured	Functional	Measured from all M-mode, and Doppler recordings
EA ratio	Peak E and A velocity ratio of mitral inflow for left ventricular diastolic function	Measured	Functional	
LVSV	Left Ventricle (LV) stroke volume	Calculated	Functional	$LVSV = \pi \cdot VTI \cdot \left(\frac{AoD}{2}\right)^2$
CO	Cardiac output	Calculated	Functional	$CO = LVSV \cdot HR$
LVFS	Left Ventricle (LV) fractional shortening	Calculated	Functional	$LVFS = 100 \cdot \frac{LVEDD - LVESD}{LVEDD}$
LV AW T	Left Ventricle (LV) anterior wall thickening (%)	Calculated	Functional	$LVAWT = 100 \cdot \frac{LVAWes - LVAWed}{LVAWed}$
LV PWT	Left Ventricle (LV) posterior wall thickening (%)	Calculated	Functional	$LVPWT = 100 \cdot \frac{LVPWes - LVPWed}{LVPWed}$

Note: The acronym, full name, and type (morphological or functional) of each measurement are given. For each measurement, the method of acquisition (termed “class”; measured or calculated) is given along with the acquisition details (how it was measured [with ultrasound imaging] or calculated).

Group effect prior of standard deviation σ_{jkm} :

$$\gamma_{jk}^1 \sim Unif(-\infty, +\infty)$$

Random effect prior:

$$\beta_{m_i} \sim \mathcal{N}\left(0, \sigma_{m_i}^2\right)$$

(B) Homoscedastic model:

$$y_i \sim \mathcal{N}\left(\mu_{j,k,m_i}, \sigma_{jk}^2\right)$$

$$\mu_{j,k,m_i} = \beta_0 + \beta_1 \cdot group_{j,k_i} + \beta_{m_i}$$

Intercept prior:

$$\beta_{j,k_i}^0 \sim Student^+(0, 2.5, 3)$$

Group effect prior:

$$\beta_{j,k_i}^1 \sim Unif(-\infty, +\infty)$$

Random effect β_{m_i} standard deviation prior:

$$\sigma_{m_i} \sim Student^+(0, 2.5, 3) \quad (1)$$

The Z-scored data for each observation (i) of every cardiac measure (j), mouse group (k) and mouse ID (m), y_i , is modeled as a normal distribution with a mean (μ_{j,k,m_i}) and a variance which either varies with measure and mouse group (σ_{jkm}^2) (heteroscedastic) or varies only with measure (σ_{jk}^2) (homoscedastic). β_{j,k_i}^0 is the intercept and β_{j,k_i}^1 is the group effect of the mean (μ_{j,k,m_i}). β_{m_i} is the random effect of mouse ID to account for repeated measurements and σ_{m_i} is the standard deviation of the normal prior on β_{m_i} . γ_{jk}^0 is the intercept and γ_{jk}^1 is the group effect of the standard deviation σ_{jkm} of y_i . $Student^+(0, 2.5, 3)$ is

the half-Student- t distribution with zero mean, scaling factor 2.5 and 3 degrees of freedom.

The comparison of the two models was performed using the pareto-smoothed-importance-sampling leave-one-out cross-validation (*PSIS LOO CS*) method (Vehtari et al., 2017) in the loo package (Vehtari et al., 2020). For each measure, we then used the model that performed the best (Table 4).

For all sets of measures, we used the posterior distribution to obtain estimates for the mean for each genetic group. However, for measures fit using the heteroscedastic model, we obtained variance (sigma) for each genetic group, while measures fit using the homoscedastic model, we obtained a single posterior distri-

Once the posterior distributions were obtained a series of comparisons were performed. Specifically, each mutant group (total of 9) was compared to the WT control group for each cardiac measure (total of 15), for a total of 135 comparisons. Additionally, each mutant group (total of 9) was compared to every other mutant group per cardiac measure (total of 15), for a total of 540 comparisons.

For each posterior distribution we obtained the following metrics: median, mean, 89% credible intervals (CIs) and probability of direction (pd ; Makowski, Ben-Shachar, Chen, & Lüdecke, 2019; Makowski, Ben-Shachar, & Lüdecke, 2019). We controlled for the false discovery rate based on methods presented by J. Storey (Storey, 2003). Firstly, we calculated the posterior error

$$PEP_{i_adjusted} = \frac{p_{prior} \cdot PEP_{i_cumulative}}{p_{prior} \cdot PEP_{i_cumulative} + (1 - p_{prior}) \cdot (1 - PEP_{i_cumulative})} \quad (2)$$

bution for the variance (sigma) shared amongst genetic groups.

TABLE 4 Type of Bayesian model used for each cardiac measure

Cardiac measure	Type of Bayesian model
Aorta diameter (AoD)	Heteroscedastic
Velocity time integral (VTI)	Homoscedastic
Peak E to A velocity ratio	Homoscedastic
Left ventricular (LV) chamber diameter (end-systole)	Heteroscedastic
Left ventricular (LV) chamber diameter (end-diastole)	Homoscedastic
Left ventricular (LV) anterior wall thickness (end-systole)	Heteroscedastic
Left ventricular (LV) anterior wall thickness (end-diastole)	Homoscedastic
Left ventricular (LV) posterior wall thickness (end-systole)	Heteroscedastic
Left ventricular (LV) posterior wall thickness (end-diastole)	Heteroscedastic
Left ventricular (LV) anterior wall thickening	Homoscedastic
Left ventricular (LV) posterior wall thickening	Heteroscedastic
Heart rate (HR)	Heteroscedastic
Cardiac output (CO)	Heteroscedastic
Left ventricular fractional shortening (LVFS)	Homoscedastic
Left ventricular stroke volume (LVSV)	Heteroscedastic

Note: One Bayesian model was run per cardiac measure comparing all genetic groups. For each model, the variance was either considered constant across genetic groups (homoscedastic) or varying between genetic groups (heteroscedastic).

probability (PEP) using: $PEP = 1 - pd$. PEP was used as a Bayesian p-value equivalent. Subsequently, we performed a correction on the PEP values using the formula:

Calculation of adjusted PEP of rank i to correct for multiple comparisons. p_{prior} is the prior estimate of the PEP value (p -value). Each $PEP_{i_cumulative}$ is obtained after ranking the PEP values in increasing order (rank given by i) and adding all PEP values of less or equal rank to get $PEP_{I_cumulative}$.

The prior estimate of the PEP value (p_{prior}) was obtained from the histogram of the PEP values (chosen bin size 0.05), using the following equation:

$$p_{prior} = \frac{N_{\{-1\}}}{N} \quad (3)$$

Estimate of prior PEP value. $N_{\{-1\}}$ is the sum of counts in all bins except for the first bin of the PEP histogram. N is the sum of counts in all bins. Chosen bin size was 0.05. $PEP_{adjusted} \leq 0.05$ was considered to be of high confidence or significant.

Principal component analysis and total correlation

Principal component analysis (PCA) and total correlation were used to explore the redundancy in our cardiac measures and genetic groups. This corresponds to comparing the genetic group by cardiac measure matrix of posterior means against its transpose. First, for visual inspection, for each data matrix orientation (original and transposed), bootstrapping with replacement was performed

to determine the median eigenvalue density for each PC component (as captured by the scree plot) along with the associated 95% confidence intervals. Second, to quantify the redundancy, total correlation was calculated (Timme et al., 2014).

Total correlation is sensitive to dimension (Timme et al., 2014). Thus, to make the total correlation comparable across both datasets, each dataset was iteratively downsampled to the lowest dimension ($N_{\text{genetic groups}} \times N_{\text{genetic groups}}$) by performing random selection without replacement of columns or rows where appropriate. For

each dataset, the mean and standard deviation of the total correlation across all iterations were calculated. Further details on the total correlation calculation can be found in the Supporting Information.

RESULTS

The type of model (heteroscedastic or homoscedastic) run per cardiac measure is shown in Table 4. Depending on the model, coefficient estimates (posterior distributions)

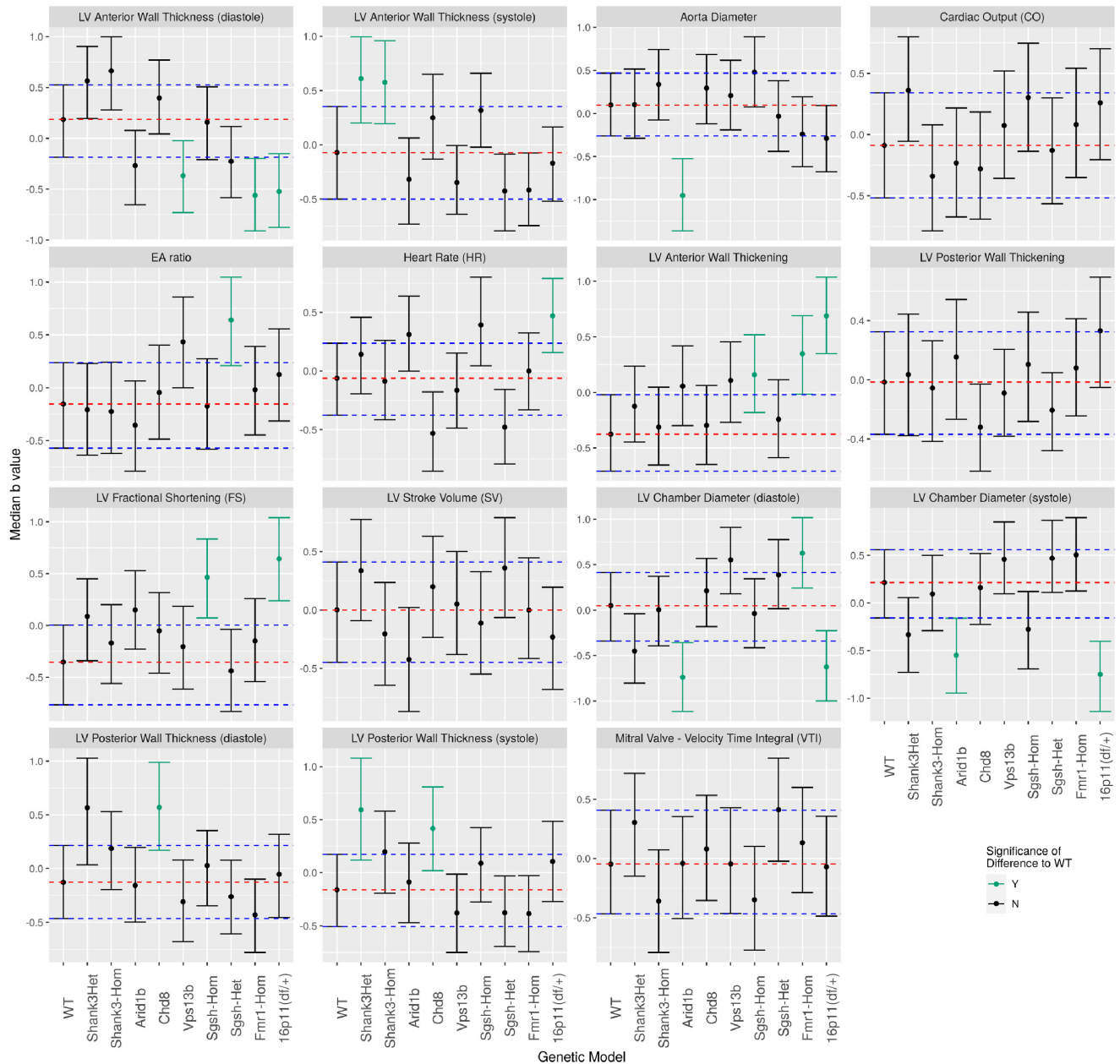


FIGURE 1 Median coefficient estimates (b -values) per genetic group per cardiac measure. Unadjusted 89% credible intervals (CIs) shown as whiskers. The blue dashed lines indicate the upper and lower 89% CIs for the WT control group. The red dashed line indicates the median of the wild-type (WT) control group. Green color indicates the groups that are significantly different from WT controls. Significance assigned based on FDR corrected q values

were obtained either only for the median or for both the median and variance of the coefficients. The coefficient estimates for the median are shown in Figure 1.

We determined the number of “high confidence” or “significant” ($PEP_{adjusted} \leq 0.05$) tests per genetic group, compared to all tests performed for that group. The fraction of high-confidence tests was used as a metric of difference compared to the reference group. The higher the fraction, the more (measures with) significant differences between the groups. Similarly, for each cardiac measure the number of high-confidence tests was calculated (relative to the total number of tests). In this case, it was interpreted as the prevalence of each cardiac measure in an abnormal cardiac phenotype. The higher the fraction, the more often would that cardiac measure be abnormal (relative to the reference group).

Comparing ASD-related genetic models to littermate wild-type controls

From our results, the differences between mutant groups and wild-type (WT) controls varied between mutant groups in both number and magnitude (Figure 2). The mutant group with the greatest number of significant differences in cardiac phenotype relative to WT controls was the 16p11.2 (deletion) group (6/15 measures) with the

Arid1b^(+/-) and *Fmr1*^(-/-) groups following (3/15 measures). Next, were the *Shank3*^(+/-) (Δ exon 4–9), *Chd8*^(+/-) and *Sgsh*^(-/-) groups (2/15 measures each but not in all the same cardiac measures; Figure 3a). In all comparisons to WT controls, the cardiac measures that were most often found abnormal were, the left ventricular (LV) anterior wall thickening (LVAWT; 3/9 groups), LV chamber diameter at end-diastole (LVEDD; 3/9 groups), and LV anterior wall thickness at end-diastole (LVAWed; 3/9 groups) and end-systole (LVAWes; 2/9 groups; Figure 3b). Overall, there were mainly morphological differences, but functional differences were also present.

Comparing ASD-related genetic mouse groups

To explore the heterogeneity amongst mutant groups, we identified the cardiac measures that differed most between groups (Figure 4a), the mutant groups with most differences from all other groups (Figure 4b), and the mutant group pairs with the most differences.

A greater number of significant differences was present between mutant groups than when mutant groups were compared to WT controls. The measures driving the inter-group variation tended to be associated more with morphological changes than functional changes

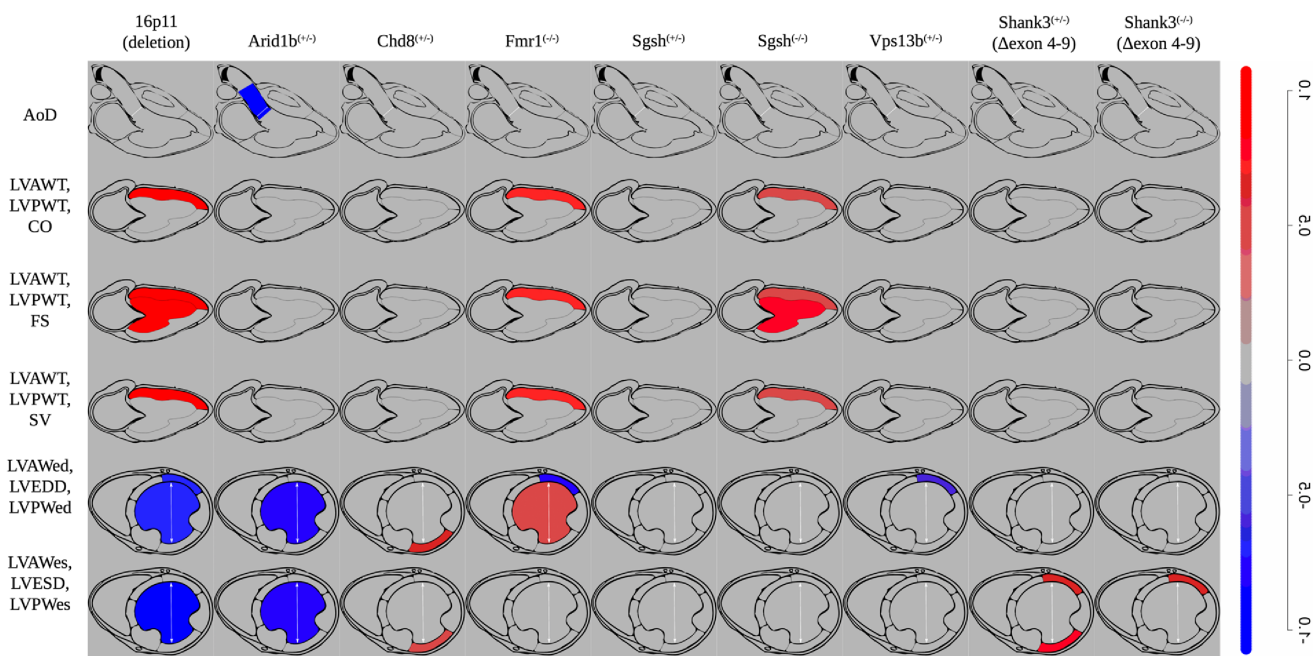


FIGURE 2 Normalized median differences per cardiac measure between each mutant mouse group and wild-type controls (WTs). The color gradient was generated mapping to the range of normalized median values; only the data from the high-confidence (significant) tests across all cardiac measures and groups were used. For all other (non-significant) tests, a gray color was assigned, same as the background. Each column corresponds to a mutant mouse group and each row depicts one or a set of cardiac measures. AoD, aorta diameter; LVAWT, left ventricular anterior wall thickening; LVPWT, left ventricular posterior wall thickening; CO, cardiac output; FS, fractional shortening; LVAWed, left ventricular end-diastolic anterior wall thickness; LVEDD, left ventricular end-diastolic (chamber) diameter; LVPW, left ventricular end-diastolic posterior wall thickness; LVAWes, left ventricular end-systolic anterior wall thickness; LVESD, left ventricular end-systolic (chamber) diameter; LVPWes, left ventricular end-systolic posterior wall thickness

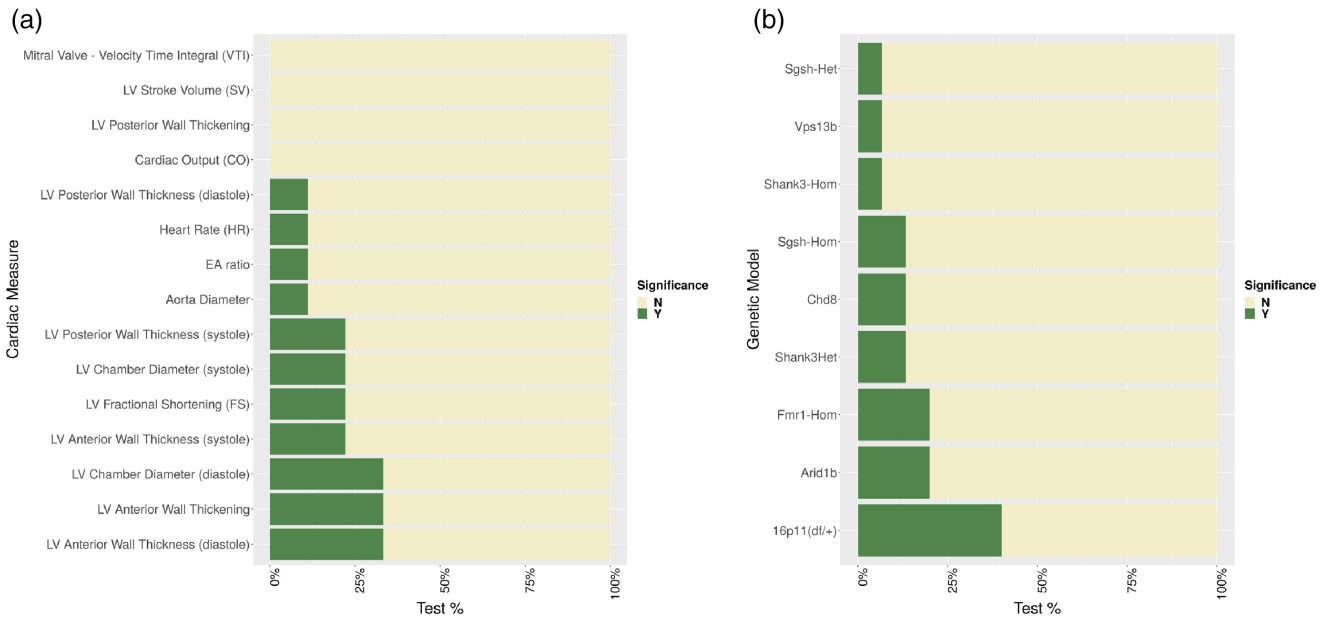


FIGURE 3 Barplots indicating the percent of significant (high confidence) comparisons (tests) between mutants and WT controls. (A) For each cardiac measure all ASD-related mutant groups were compared to WT controls; the same total number of comparisons (tests) was conducted for all cardiac measures. The green bar indicates the percent of significant comparisons (tests) for each cardiac measure. (B) Similar to (A), each ASD-related mutant group was compared to WT controls for all cardiac measures; same number of comparisons (tests) was conducted for all mutant groups. The green bar indicates the percent of significant comparisons (tests) for each group. ASD, autism spectrum disorder; WT, wild-type

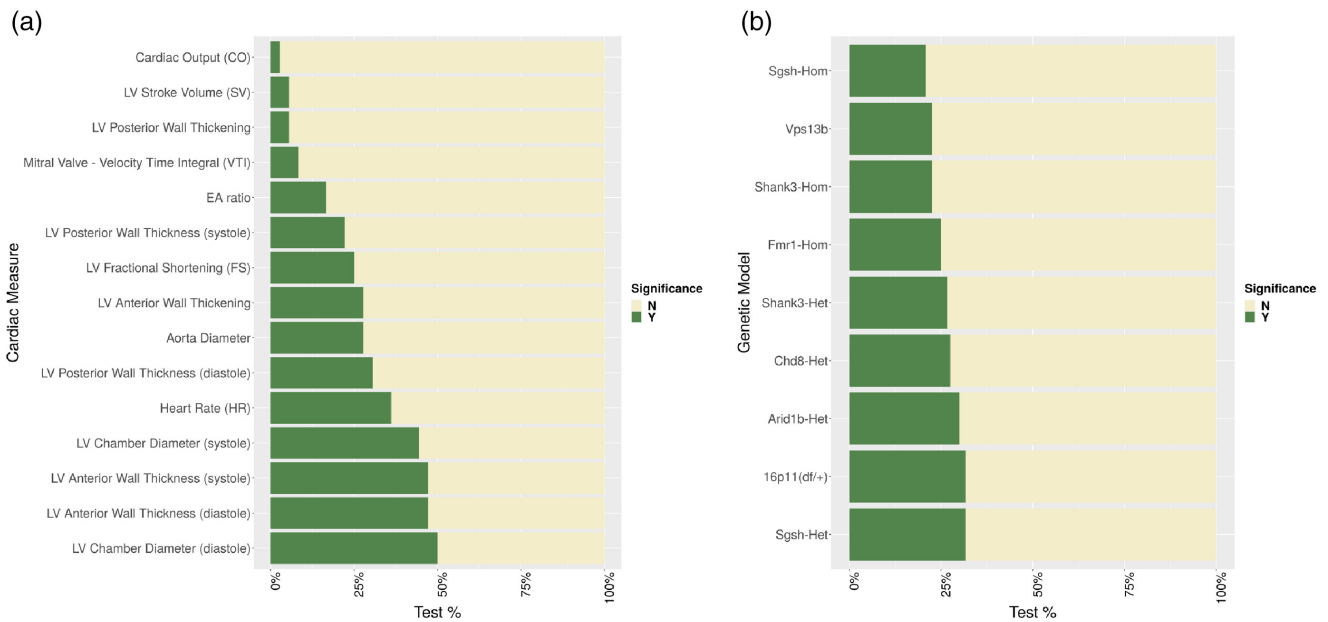


FIGURE 4 Barplots indicating the percent of significant (high confidence) comparisons (tests) between all autism spectrum disorder (ASD)-related genetic mutant groups. (A) For each cardiac measure all ASD-related mutant groups were compared to each other; the same total number of comparisons (tests) was conducted for all cardiac measures. The green bar indicates the percent of significant comparisons (tests) for each cardiac measure. (B) Similar to (A), each ASD-related mutant group was compared to every other mutant group, for all cardiac measures; same number of comparisons (tests) was conducted for all mutant groups. The green bar indicates the percent of significant comparisons (tests) for each group

(Figure 4a). Specifically, the mutant groups firstly differ in LV chamber diameter at end-diastole (LVEDD; significance found in 18/138 pairwise comparisons) and, secondly, in LV anterior wall thickness at end-systole and

end-diastole (LVAWes, LVAWed; 17/138 pairwise comparisons each). Third, they differ in LV chamber diameter at end-systole (LVESD; 16/138 pairwise comparisons), followed by heart rate (HR) (13/138 pairwise

TABLE 5 Total correlation values per dataset

	Total correlation original dimensions	Total correlation downsampled data	Total correlation downsampled data standard deviation
Original—Cardiac Measures	66.18	18.15	1.3
Original—Genetic Groups	10.79	19.36	1.26

Note: First column is the total correlation of the original datasets. In the second and third column are the mean total correlation and standard deviation respectively, across all iterations, for the downsampled data.

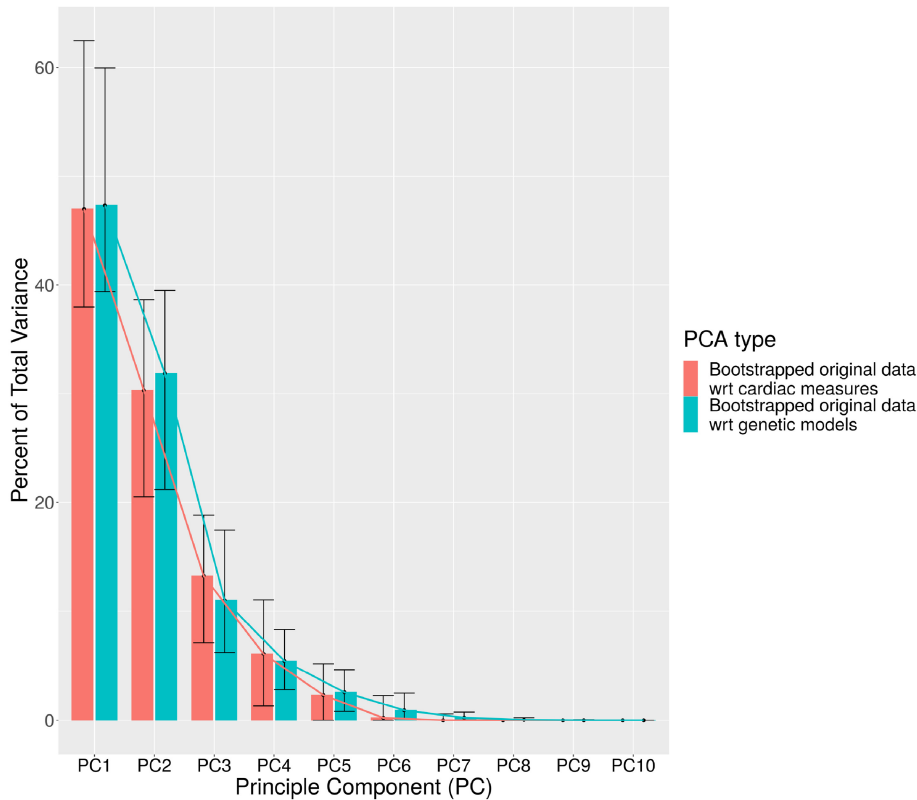


FIGURE 5 Scree plot of principal component analysis (PCA) on cardiac measures and PCA on genetic models. Bootstrapping with replacement of the data was performed to determine the median eigenvalue density for each PC component along with the associated 95% confidence intervals. The bootstrapped data are shown along with the bootstrapped median values and 95% confidence intervals. The estimated decay curve is also mapped

comparisons). The 16p11.2 (deletion) and *Sgsh*^(+/-) groups had the most differences from all other mutant groups (38/1080 pairwise comparisons), followed by the *Arid1b*^(+/-) (36/120 pairwise comparisons) and *Chd8*^(+/-) (33/120 pairwise comparisons) groups (Figure 4b).

Conducting pairwise mutant group analysis, the *Shank3*^(+/-) (Δ exon 4–9) - *Sgsh*^(+/-) and the *Chd8*^(+/-) - 16p11.2 (deletion) pairs had the greatest number of significant differences in cardiac measures (8/15 measures), followed by the *Shank3*^(-/-) (Δ exon 4–9) - 16p11.2 (deletion) and *Arid1b*^(+/-) - *Sgsh*^(+/-) pairs (7/15 measures each).

Of interest is the comparison of the distributions in Figures 3a and 4a. When compared to each other, mutant groups tended to differ more in morphological measures than in functional measures (Figure 4a), but when compared to WT controls, they tended to differ roughly equally in both (Figure 3a).

Principal component analysis and total correlation

For the 15 cardiac measures, PCA revealed that 9 principal components were required to account for ~99% of the variance in the data (Figure 5). This can be explained by the fact that, from the set of 15 measures, 5 were not directly measured but were calculated using others, as described in Methods. For the 10 genetic groups, PCA also revealed that 9 principal components were required to account for ~99% of the variance in the data (Figure 5). Therefore, there does not seem to be any pattern of similarity (redundancy) between the mutant groups with regard to cardiac phenotype.

To inspect the comparable redundancy between cardiac measures and genetic groups, the total correlation was computed (Table 5). The total correlation of 15 cardiac measures was 66.18 and of 10 genetic groups was 10.79. As total correlation is sensitive to the number of

dimensions, we randomly downsampled both datasets to 10 dimensions with 1000 permutations (reporting mean \pm standard deviation). The total correlation of the downsampled cardiac measures was 18.15 ± 1.3 and of the downsampled genetic groups was 19.36 ± 1.26 . Thus, the total correlation, and therefore redundancy, is comparable between cardiac measures and genetic groups. Among cardiac measures and amongst genetic groups, respectively, some redundancy or correlation exists since for random data the total correlation would be zero.

DISCUSSION

Our analysis revealed small-scale alterations in cardiac structure and function in ASD compared to WT, mirroring the clinical reports. However, significant differences of note were present. Firstly, the alterations each mutant group presented to WT controls were largely not consistent between groups. Therefore, the heterogeneity characterizing ASD in other phenotypes (Amaral, 2011; Amaral et al., 2011) is recapitulated here. Specifically, when compared to each other, mutant groups presented a greater number of significant differences than when compared to WT controls. As mentioned, this is possible due to certain mutant groups differing insignificantly from WT controls in an opposite fashion (for the same cardiac measure). Secondly, mutant groups tended to differ primarily in measures of LV structure, while when compared to WT controls, they tended to differ in both morphological and functional measures, with a small prevalence of the former. However, there was overlap in the overall associated measures with HR and LV chamber diameter and anterior wall thickness being strong contributors in both cases. Moving forward, it would be of interest to expand this work to include more ASD-related genetic models and further assess the emerging patterns.

Given the heterogeneity observed, it is valuable to determine how it compares to a standardized categorization of our genetic groups. One such categorization can be found in the SFARI Gene database (Simons Foundation: <http://gene.sfari.org/>; Banerjee-Basu & Packer, 2010) which has assigned a score to each genetic variant quantifying how closely each genetic group is linked to ASD. According to the SFARI Gene database, the 16p11.2 (deletion), *Arid1b*^(+/-), *Fmr1*^(-/-), *Shank3* (Δ exon 4–9), *Chd8*^(+/-), *Vps13b*^(+/-) groups hold a high score and the *Sgsh* group holds a lower score. However, even when assessing our results with the SFARI score in mind, a pattern cannot be identified. As shown in Figure 3b, considering the number of differences to WT controls, certain groups with a high SFARI score rank high (16p11.2 (deletion), *Arid1b*^(+/-), *Fmr1*^(-/-), *Shank3* (Δ exon 4–9)), while others rank low (*Chd8*^(+/-), *Vps13b*^(+/-)). The *Sgsh* group with a low SFARI score ranks somewhere between the two. This discrepancy between SFARI gene score and severity of cardiac

phenotype in each group could be driven by different expression levels of the associated gene between the brain and the heart.

Consequently, it seems unfeasible, with this type of assessment, to identify an overarching ASD-related cardiac phenotype, shared between all individual genetic mutant groups and setting them apart from WT controls. It seems more likely that there would be subgroups of ASD-related models, potentially not based on how closely they are linked to ASD (SFARI Gene score), each with a different cardiac phenotype compared to WT controls.

Using the results in Figure 3b on the ranking of our models with respect to number of significant differences to WTs, we can hypothesize on underlying patterns. 16p11.2 (deletion) has markedly more differences to WT than the others, both structural and functional. This could be related to the fact that the 16p11.2 locus encompasses more than one gene involved in cardiac development and function (*BCKDK*, *MAPK3*, *SRCAP*; Ghebranious et al., 2007; Sun & Wang, 2016; Wang, 2007; Xie et al., 2019; Xu et al., 2021).

Next *Arid1b*^(+/-) and *Fmr1*^(-/-) rank together. From our results, *Arid1b*^(+/-) present a decrease in aorta diameter and LV chamber diameter. *Fmr1*^(-/-) also present changes in LV chamber diameter (increase) and anterior LV wall thickness (decrease). One possible converging pathway underlying these observations is the Wnt/ β -catenin signaling pathway. *Fmr1* interacts with BMP (bone morphogenetic protein) signaling pathway, which in turn affects the Wnt signaling pathway (Kumar et al., 2019), while *Arid1b* loss-of-function mutations have been found to upregulate the Wnt/ β -catenin signaling pathway (Vasileiou et al., 2015). Additionally, *Arid1b* has also been identified as an *Fmr1* target in both NPCs and neurons (Li et al., 2020). Studies in the mouse have shown β -catenin contributes to the regulation of postnatal hypertrophic growth by acting upstream of fibroblast growth factor (FGF) signaling (Cotney et al., 2015). FGF signaling regulates second heart field (SHF) progenitors, which give rise to the atrial, ventricular and outflow tract structures (Cohen et al., 2008; Hubert et al., 2018).

Second in rank come the *Shank3*^(+/-), *Sgsh*^(-/-) and *Chd8* groups. They all present changes in LV anterior wall thickness and thickening. A possible underlying mechanism is autonomic dysregulation. The brain controls the function of the heart through neuronal pathways which involve multi-synaptic connections between the myocardial cells and peripheral ganglionic neurons, central preganglionic and premotor neurons, as part of the autonomic nervous system (sympathetic and parasympathetic regulation; Gordan et al., 2015; Silvani et al., 2016). Furthermore, a disruption in autonomic activity has been found to contribute to alteration in LV structure (Greenwood et al., 2001; Kelm et al., 1996; Patel et al., 1991; Schlaich et al., 2003). *Shank3*^(+/-),

Sgsh^(-/-) and Chd8 seem to all play a role in synaptic function. Sgsh encodes N-Sulfoglucosamine Sulfohydrolase which is involved in the lysosomal degradation of heparan sulfate (HS). HS has been found to affect neurexin and neuroligin function, indirectly impacting synaptic organization (Zhang et al., 2018). Shank3 is highly involved in synaptic function as it is a member of the ProSAP/Shank family of postsynaptic scaffolding proteins (Boeckers et al., 2002). Altered synaptic function has been documented in Shank3 (exon 4–9) knock-out mice (Jaramillo et al., 2016). Chd8 has been found to regulate directly and indirectly other genes implicated, amongst others, in synaptic function, including Shank3 (Ellingford et al., 2021; Sugathan et al., 2014). We can therefore hypothesize that in the Shank3^(+/-), Sgsh^(-/-) and Chd8 groups the changes LV wall thickness and thickening we observe result from synaptic dysfunction impacting autonomic regulation of the heart. An additional interesting hint of a common underlying mechanism is the clustering of Shank3^(+/-) and Sgsh^(-/-) based on functional MRI patterns (Zerbi et al., 2021).

Interestingly the Sgsh^(+/-) presents no significant differences to WTs. The hypothesized dysregulation may be dampened out by the presence of the one gene copy.

Finally, the Shank3^(-/-) and Vps13b^(+/-) groups present the fewest differences to WTs. Specifically, they also present a change in LV wall thickness. We can again hypothesize these LV changes are driven by autonomic dysregulation, as both Shank3^(-/-) and Vps13b^(+/-) can impact synaptic function (Greenwood et al., 2001; Kelm et al., 1996; Patel et al., 1991; Schlaich et al., 2003). Specifically, Vps13b encodes a transmembrane protein that may function in vesicle-mediated transport and sorting of proteins within the cell (Banerjee-Basu & Packer, 2010). Enrichment analysis revealed high expression in neurons and oligodendrocytes, involved mainly in synaptic function (Human Protein Atlas, n.d.; Karlsson et al., 2021; Human Protein Atlas: www.proteinatlas.org). Additionally synaptic dysfunction has been identified in iPSC-derived neurospheres and forebrain-like glutamatergic neurons of Cohen syndrome patient (Lee et al., 2020). The possible pathway in Shank3 is mentioned above (Boeckers et al., 2002; Jaramillo et al), although it is not clear how the observed effect would differ between Homozygote and Heterozygote cases.

Knowing the abnormalities present, allows us to choose alternate measures to explore more closely the observed changes and probe the underlying mechanisms. Additionally, categorizing measures as morphological or functional can offer insight about common etiology of the models' cardiac phenotype. For example, the Sinoatrial Node (SAN) is the principal pacemaker of the heart, it is characterized by cellular heterogeneity and its formation and function are controlled by a series of upstream factors (Liang et al., 2021; Wiese et al., 2009). Its cells have been clustered based on their downstream

function, revealing a wide range of targets (Liang et al., 2021). We could then hypothesize that a disruption affecting the formation of SAN (starting at embryonic day 9.5) could result in a spectrum of functional abnormalities across various genetic groups (depending on the origin and type of the disruption). Similarly for structural abnormalities.

The cardiac phenotype of each of our ASD mouse mutant groups was consistent with results seen in the corresponding human population to the extent that a direct comparison is possible (see Supporting Information). In the *Arid1b*^(+/-) group, we observed arterial stenosis at the level of the aortic valve, in agreement with clinical reports (de Rubeis & Buxbaum, 2015; Pierpont et al., 2018). In the Shank3 (exon 4–9) group we observed myocardial changes (increased anterior and posterior wall thickness) which is consistent with the reported role of Shank3 in myocardial remodeling (in mice; Cusmano-ozog et al., 2007; Lim et al., 1999; Man et al., 2020). Our findings could also be a downstream effect of patent ductus arteriosus (PDA), septal defects or right heart dysfunction, all of which have been reported (Phelan & McDermid, 2012; Pierpont et al., 2018).

The 16p11.2 (deletion) presents most abnormalities compared to WTs, which can be explained by the fact that the 16p11.2 locus encompasses more than one gene involved in cardiac development and function (*BCKDK*, *MAPK3*, *SRCAP*; Ghebranious et al., 2007; Sun & Wang, 2016; Wang, 2007; Xie et al., 2019; Xu et al., 2021). More specifically, our findings of altered anterior wall thickness and thickening, HR and fractional shortening can be effects of Tetralogy of Fallot, pulmonary atresia or aortic valve abnormalities, all reported in the literature (Pierpont et al., 2018). *Fmr1*, has the second most abnormalities, both structural (LV chamber diameter, anterior wall) and functional (anterior wall thickening) which can be anticipated by the range of abnormalities reported in literature along with the fact that CHD has been reported (<10% of cases; Berry-Kravis et al., 2019; Ciaccio et al., 2017; Ornoy et al., 2016; Pierpont et al., 2018; Tassanakijpanich et al., 2020). In the Chd8^(+/-) group, we observed increase in the LV anterior wall. Chd8 has been implicated in heart development with hypertrophy being one of the abnormalities reported, which would explain our findings (Batsukh et al., 2010; Cohen et al., 2008; Cotney et al., 2015; Hubert et al., 2018; Shanks et al., 2012). Sgsh has few reports of cardiac abnormalities, mainly systolic dysfunction, as well as valvular and septal defects (Dangel, 1998; Marques Ribeiro et al., 2014; Nijmeijer et al., 2019). A similar image is seen in our findings where we find mainly functional changes, and more so in the Homozygote (-/-) case. Finally, for the Vps13b^(+/-) group, literature reports of cardiac abnormalities speak of usually normal heart function with some cases of cardiomyopathy with decreased LV

function with age murmurs (Kivitie-Kallio et al., 1999; Kivitie-kallio & Norio, 2001; Rodrigues et al., 2018). This is recapitulated in our results where we only find altered LV anterior wall thickness.

Finally, PCA and total correlation comparison revealed a comparable redundancy between the cardiac measures and the genetic groups, while ensuring the outcome was not solely driven by underlying noise. One would expect cardiac measures to have a larger redundancy (since all measures are related to the heart), compared to the genetic groups (each was created to carry a different genetic modification). However, this result indicates that the cardiac measures used in this study are more independent than one would expect (with some correlation amongst them still present). Thus, once again, confirming that our UBM protocol captures various dimensions of cardiac functionality, as intended, and can be used as an effective screening protocol. For the genetic groups, this result indicates there is some correlation between the ASD-related models but overall, as mentioned previously, the heterogeneity characteristic of ASD is recapitulated in the cardiac phenotype as well.

There are certain limitations to this work, which must be considered. First, this work was conducted using adult mice. However, various genetically driven cardiac abnormalities, and especially CHD, occur early in life. So, by screening in adult age, there is a risk of observing a modified state which resulted from various adaptive mechanisms acting throughout development. Second, only male mice were used in the study. Given the known sex differences in ASD (Loomes et al., 2017) and cardiac function (Regitz-Zagrosek & Kararigas, 2017), we recognize it may be of value to repeat this work on female mice. Thirdly, the downsampling procedure used for the calculation of total correlation is not a standard approach for comparing two datasets of differing dimensions. So further investigation is needed to verify this approach. Finally, a direct comparison between our results and the clinical literature is not possible because clinical studies often employ different study designs (assessment protocols, sample sizes, etc.) and recruit both male and female patients. Namely, in this study we did not perform direct assessment of the atrioventricular septum, the right side of the heart, the extracardiac space or the conduction system of the heart, which are widely mentioned in many of the clinical reports, as is shown in Tables S1 and S2. However, potential links can be inferred based on knowledge of the overall structure and function of the cardiovascular system. As the number of ASD-related genetic models screened with this protocol increases and as the corresponding clinical data amounts, we will be able to make even more concrete comparisons. Finally, we should caution about the translatability of our results to other ASD genetic subtypes. Even more, we must stress the possible lack of translatability to cases of idiopathic ASD where a genetic cause has not been identified and

thus no association exists with any of these or other genes.

In conclusion, this work sheds light on the spectrum of cardiac abnormalities associated with ASD-related genetic abnormalities. The heterogeneity characterizing ASD in other phenotypes is recapitulated here, with more differences seen between mutant groups than when compared to WT. Alterations were small in scale, but significant, and further exploration of more models is needed to validate the observed patterns. Our high frequency ultrasound imaging protocol as a method of cardiac assessment provides a well-rounded view of cardiac structure and function, effectively capturing the clinically reported cardiac abnormalities. Thus, it can be used as a screening protocol moving forward. The detected cardiac abnormalities can then be further examined using potentially more sensitive methods to explore their underlying mechanisms. By classifying cardiac measures as morphological or functional, the etiology of mutant phenotype can be better understood, and any common underlying mechanisms can be elucidated. Clinically, knowledge of the cardiac abnormalities associated with ASD can be greatly beneficial as, even non-lethal cardiac abnormalities can impact the normal development and function of various other biological systems, such as the brain. In addition, the presence of specific cardiac abnormalities may provide mechanistic insights for a patient's ASD subtype.

ACKNOWLEDGMENTS

The authors wish to acknowledge Maria Robles for her help with colony management and technical support. This work was supported by funding from the Canadian Institute of Health Research. Stephania Assimopoulos was supported by a Restracom Fellowship funded by the Hospital for Sick Children and an Ontario Graduate Scholarship.

CONFLICT OF INTEREST

The authors declare no conflict of interest.

AUTHOR CONTRIBUTIONS

Stephania Assimopoulos: Conception and design of the work, acquisition, analysis, and interpretation of data. Creation of software used in the work. Writing of the manuscript. **Christopher Hammill:** Analysis, and interpretation of data. **Darren J. Fernandes:** Analysis, and interpretation of data. **Tara Leigh Spencer Noakes:** Training on experimental methods used for data acquisition. **Yu-Qing Zhou:** Development and training on experimental methods used for data acquisition. **Lauryl M. J. Nutter:** Creation of the genetic mouse models used in the study. **Jacob Ellegood:** Contribution to creation of the genetic mouse models used in the study. **Evdokia Anagnostou:** Conception of the work. Substantive revision of the manuscript. **John G. Sled:** Conception of the work. **Jason P. Lerch:** Conception and design of the work, interpretation of data, and substantive revision of the manuscript.

DATA AVAILABILITY STATEMENT

The data that support the findings of this study are available on request from the corresponding author. The data are not publicly available due to privacy or ethical restrictions.

ETHICS STATEMENT

All procedures involving animals were performed in compliance with the Animals for Research Act of Ontario and the Guidelines of the Canadian Council on Animal Care. The Centre for Phenogenomics (TCP) Animal Care Committee reviewed and approved all procedures conducted on animals at TCP.

ORCID

Stephania Assimopoulos  <https://orcid.org/0000-0002-7321-6297>

Christopher Hammill  <https://orcid.org/0000-0001-9823-2827>

Lauryl M. J. Nutter  <https://orcid.org/0000-0001-9619-146X>

REFERENCES

- Acampa, M., & Guideri, F. (2006). Cardiac disease and Rett syndrome. *Archives of Disease in Childhood*, *91*(5), 440–443. <https://doi.org/10.1136/adc.2005.090290>
- Amaral, D., Dawson, G., & Geschwind, D. (2011). *Autism Spectrum Disorders*. Oxford University Press <https://books.google.ca/books?id=Prf0InCqQS0C>
- Amaral, D. G. (2011). The promise and the pitfalls of autism research: An introductory note for new autism researchers. *Brain Research*, *1380*(916), 3–9. <https://doi.org/10.1016/j.brainres.2010.11.077>
- Banerjee-Basu, S., & Packer, A. (2010). SFARI gene: An evolving database for the autism research community. *DMM Disease Models and Mechanisms*, *3*(3–4), 133–135. <https://doi.org/10.1242/dmm.005439>
- Batsukh, T., Pieper, L., Koszucka, A. M., von Velsen, N., Hoyerfender, S., Elbracht, M., Bergman, J. E. H., Hoefsloot, L. H., & Pauli, S. (2010). CHD8 interacts with CHD7, a protein which is mutated in CHARGE syndrome. *Human Molecular Genetics*, *19*(14), 2858–2866. <https://doi.org/10.1093/hmg/ddq189>
- Benevides, T. W., & Lane, S. J. (2013). A review of cardiac autonomic measures: Considerations for examination of physiological response in children with autism Spectrum disorder. *Journal of Autism and Developmental Disorders*, *45*(2), 560–575. <https://doi.org/10.1007/s10803-013-1971-z>
- Berry-Kravis, E., Hipp, H., Hunter, J. E., Saul, R. A., Tarleton, J. C., & Todd, P. K. (2019). FMR1 Disorders. In R. Pagon, M. Adam, H. Ardinger, S. Wallace, A. Amemiya, L. Bean, T. Bird, N. Ledbetter, H. Mefford, R. Smith, & K. Stephens (Eds.), *GeneReviews*. GeneReviews <http://europepmc.org/article/NBK/NBK1116>
- Blake, K. D., & Prasad, C. (2006). CHARGE syndrome. *Orphanet Journal of Rare Diseases*, *1*(1), 1–8. <https://doi.org/10.1186/1750-1172-1-34>
- Boczek, N. J., Ye, D., Jin, F., Tester, D. J., Huseby, A., Bos, J. M., Johnson, A. J., Kanter, R., & Ackerman, M. J. (2015). Identification and functional characterization of a novel CACNA1C-mediated cardiac disorder characterized by prolonged QT intervals with hypertrophic cardiomyopathy. Congenital heart defects, and sudden cardiac death. *Circulation: Arrhythmia and Electrophysiology*, *8*(5), 1122–1132. <https://doi.org/10.1161/CIRCEP.115.002745>
- Boeckers, T. M., Bockmann, J., Kreutz, M. R., & Gundelfinger, E. D. (2002). ProSAP/Shank proteins—A family of higher order organizing molecules of the postsynaptic density with an emerging role in human neurological disease. *Journal of Neurochemistry*, *81*(5), 903–910. <https://doi.org/10.1046/j.1471-4159.2002.00931.x>
- Bozdagi, O., Sakurai, T., Papapetrou, D., Wang, X., Dickstein, D. L., Takahashi, N., Kajiwara, Y., Yang, M., Katz, A. M., Scattoni, M. L., Harris, M. J., Saxena, R., Silverman, J. L., Crawley, J. N., Zhou, Q., Hof, P. R., & Buxbaum, J. D. (2010). Haploinsufficiency of the autism-associated Shank3 gene leads to deficits in synaptic function, social interaction, and social communication. *Molecular Autism*, *1*, 1–15. <https://doi.org/10.1186/2040-2392-1-15>
- Bujnakova, I., Ondrejka, I., Mestanik, M., Visnovcova, Z., Mestanikova, A., Hrtanek, I., Fleskova, D., Calkovska, A., & Tonhajzerova, I. (2016). Autism spectrum disorder is associated with autonomic underarousal. *Physiological Research*, *65*, S673–S682. <https://doi.org/10.33549/physiolres.933528>
- Bürkner, P. C. (2017). brms: An R package for Bayesian multilevel models using Stan. *Journal of Statistical Software*, *80*(1), 1–28. <https://doi.org/10.18637/jss.v080.i01>
- Bürkner, P. C. (2018). Advanced Bayesian multilevel modeling with the R package brms. *The R Journal*, *10*, 395–411. <https://doi.org/10.32614/RJ-2018-017>
- Chandler, N., Aslanidi, O., Buckley, D., Inada, S., Birchall, S., Atkinson, A., Kirk, D., Monfredi, O., Molenaar, P., Anderson, R., Sharma, V., Sigg, D., Zhang, H., Boyett, M., & Dobrzynski, H. (2011). Computer three-dimensional anatomical reconstruction of the human sinus node and a novel Paranodal area. *Anatomical Record*, *294*(6), 970–979. <https://doi.org/10.1002/ar.21379>
- Ciaccio, C., Fontana, L., Milani, D., Tabano, S., Miozzo, M., & Esposito, S. (2017). Fragile X syndrome: A review of clinical and molecular diagnoses. *Italian Journal of Pediatrics*, *43*(1), 1–12. <https://doi.org/10.1186/s13052-017-0355-y>
- Clouchoux, C., Kudelski, D., Gholipour, A., Warfield, S. K., Viseur, S., Bouyssi-Kobar, M., Mari, J. L., Evans, A. C., du Plessis, A. J., & Limperopoulos, C. (2012). Quantitative in vivo MRI measurement of cortical development in the fetus. *Brain Structure and Function*, *217*(1), 127–139. <https://doi.org/10.1007/s00429-011-0325-x>
- Cohen, E. D., Tian, Y., & Morrisey, E. E. (2008). Wnt signaling: An essential regulator of cardiovascular differentiation, morphogenesis and progenitor self-renewal. *Development*, *135*(5), 789–798. <https://doi.org/10.1242/dev.016865>
- Corsten-Janssen, N., Kerstjens-Frederikse, W. S., du Marchie Sarvaas, G. J., Baardman, M. E., Bakker, M. K., Bergman, J. E. H., Hove, H. D., Heimdal, K. R., Rustad, C. F., Hennekam, R. C. M., Hofstra, R. M. W., Hoefsloot, L. H., van Ravenswaaij-Arts, C. M. A., & Kapusta, L. (2013). The cardiac phenotype in patients with a CHD7 mutation. *Circulation: Cardiovascular Genetics*, *6*(3), 248–254. <https://doi.org/10.1161/CIRCGENETICS.113.000054>
- Cotney, J., Muhle, R. A., Sanders, S. J., Liu, L., Willsey, A. J., Niu, W., Liu, W., Klei, L., Lei, J., Yin, J., Reilly, S. K., Tebbenkamp, A. T., Bichsel, C., Pletikos, M., Sestan, N., Roeder, K., State, M. W., Devlin, B., & Noonan, J. P. (2015). The autism-associated chromatin modifier CHD8 regulates other autism risk genes during human neurodevelopment. *Nature Communications*, *6*, 6404. <https://doi.org/10.1038/ncomms7404>
- Croen, L. A., Zerbo, O., Qian, Y., Massolo, M. L., Rich, S., Sidney, S., & Kripke, C. (2015). The health status of adults on the autism spectrum. *Autism*, *19*(7), 814–823. <https://doi.org/10.1177/1362361315577517>
- Cusmano-ozog, K., Manning, M. A., & Hoyme, H. E. (2007). 22q13.3 deletion syndrome: A recognizable malformation syndrome associated with marked speech and language delay. *American Journal of Medical Genetics*, *145*, 393–398. <https://doi.org/10.1002/ajmg.c>

- Dangel, J. H. (1998). Cardiovascular changes in children with mucopolysaccharide storage diseases and related disorders - clinical and echocardiographic findings in 64 patients. *European Journal of Pediatrics*, *157*, 534–538.
- Dawson, S., Glasson, E. J., Dixon, G., & Bower, C. (2009). Birth defects in children with autism spectrum disorders: A population-based, nested case-control study. *American Journal of Epidemiology*, *169*(11), 1296–1303. <https://doi.org/10.1093/aje/kwp059>
- de Felice, C., Maffei, S., Signorini, C., Leoncini, S., Lunghetti, S., Valacchi, G., D'Esposito, M., Filosa, S., Ragione, F., Butera, G., Favilli, R., Ciccoli, L., & Hayek, J. (2012). Subclinical myocardial dysfunction in Rett syndrome. *European Heart Journal Cardiovascular Imaging*, *13*(4), 339–345. <https://doi.org/10.1093/ejehocard/jer256>
- de Rubeis, S., & Buxbaum, J. D. (2015). Genetics and genomics of autism spectrum disorder: Embracing complexity. *Human Molecular Genetics*, *24*(R1), R24–R31. <https://doi.org/10.1093/hmg/ddv273>
- Debbané, M., Fountain, D. M., Mutlu, A. K., Eliez, S., Schaer, M., & Schneider, M. (2014). Congenital heart disease is associated with reduced cortical and hippocampal volume in patients with 22q11.2 deletion syndrome. *Cortex*, *57*, 128–142. <https://doi.org/10.1016/j.cortex.2014.04.004>
- Doevendans, P. A., Daemen, M. J., de Muinck, E. D., & Smits, J. F. (1998). Cardiovascular phenotyping in mice. *Cardiovascular Research*, *39*(1), 34–49. [https://doi.org/10.1016/S0008-6363\(98\)00073-X](https://doi.org/10.1016/S0008-6363(98)00073-X)
- Doshi-Velez, F., Ge, Y., & Kohane, I. (2014). Comorbidity clusters in autism spectrum disorders: An electronic health record time-series analysis. *Pediatrics*, *133*(1), e54–e63. <https://doi.org/10.1542/peds.2013-0819>
- Ellegood, J., & Crawley, J. N. (2015). Behavioral and neuroanatomical phenotypes in mouse models of autism. *Neurotherapeutics*, *12*(3), 521–533. <https://doi.org/10.1007/s13311-015-0360-z>
- Ellingford, R. A., Panasiuk, M. J., de Meritens, E. R., Shaunak, R., Naybour, L., Browne, L., Basson, M. A., & Andraea, L. C. (2021). Cell-type-specific synaptic imbalance and disrupted homeostatic plasticity in cortical circuits of ASD-associated Chd8 haploinsufficient mice. *Molecular Psychiatry*, *26*(7), 3614–3624. <https://doi.org/10.1038/s41380-021-01070-9>
- Foster, F. S., Mehi, J., Lukacs, M., Hirson, D., White, C., Chaggares, C., & Needles, A. (2009). A new 15-50 MHz array-based micro-ultrasound scanner for preclinical imaging. *Ultrasound in Medicine and Biology*, *35*(10), 1700–1708. <https://doi.org/10.1016/j.ultrasmedbio.2009.04.012>
- Gabry, J., & Goodrich, B. (2017). *rstanarm: Bayesian Applied Regression Modeling via Stan*. (R package version 2.15.3). <https://mc-stan.org/rstanarm>
- Gabry, J., Simpson, D., Vehtari, A., Betancourt, M., & Gelman, A. (2019). Visualization in Bayesian workflow. *Journal of the Royal Statistical Society. Series A: Statistics in Society*, *182*(2), 389–402. <https://doi.org/10.1111/rssa.12378>
- Gaynor, J. W., Wernovsky, G., Jarvik, G. P., Bernbaum, J., Gerdes, M., Zackai, E., Nord, A. S., Clancy, R. R., Nicolson, S. C., & Spray, T. L. (2007). Patient characteristics are important determinants of neurodevelopmental outcome at one year of age after neonatal and infant cardiac surgery. *Journal of Thoracic and Cardiovascular Surgery*, *133*(5), 1344–1353. <https://doi.org/10.1016/j.jtcvs.2006.10.087>
- Gelman, A. (2013). Bayesian data analysis Gelman. *Journal of Chemical Information and Modeling*, *53*, 9.
- Ghebranious, N., Giampietro, P. F., Wesbrook, P., & Rezkalla, S. H. (2007). A novel microdeletion at 16p11.2 harbors candidate genes for aortic valve development, seizure disorder, and mild mental retardation. *American Journal of Medical Genetics/genetics*, *143*, 1462–1471. <https://doi.org/10.1002/ajmg.a>
- Gordan, R., Gwathmey, J. K., & Xie, L.-H. (2015). Autonomic and endocrine control of cardiovascular function. *World Journal of Cardiology*, *7*(4), 204–214. <https://doi.org/10.4330/wjcv7.i4.204>
- Greenwood, J. P., Scott, E. M., Stoker, J. B., & Mary, D. A. S. G. (2001). Hypertensive left ventricular hypertrophy: Relation to peripheral sympathetic drive. *Journal of the American College of Cardiology*, *38*(6), 1711–1717. [https://doi.org/10.1016/S0735-1097\(01\)01600-X](https://doi.org/10.1016/S0735-1097(01)01600-X)
- Habib, G. B., & Zoghbi, W. A. (1992). Doppler assessment of right ventricular filling dynamics in systemic hypertension: Comparison with left ventricular filling. *American Heart Journal*, *124*(5), 1313–1320. [https://doi.org/10.1016/0002-8703\(92\)90417-T](https://doi.org/10.1016/0002-8703(92)90417-T)
- Hagerman, R., Hoem, G., & Hagerman, P. (2010). Fragile X and autism: Intertwined at the molecular level leading to targeted treatments. *Molecular Autism*, *1*(1), 1–14. <https://doi.org/10.1186/2040-2392-1-12>
- Hamlin, R. L., & Altschuld, R. A. (2011). Extrapolation from mouse to man. *Circulation: Cardiovascular Imaging*, *4*(1), 2–4. <https://doi.org/10.1161/CIRCIMAGING.110.961979>
- Henk Van Der Tweel, L., Strackee, J., Stokhof, A. A., Wassenaar, C., & Meijler, F. L. (1999). ECG of the “newborn” mouse (mus domesticus) with specific reference to comparative AV transmission. *Journal of Cardiovascular Electrophysiology*, *10*(2), 168–173. <https://doi.org/10.1111/j.1540-8167.1999.tb00658.x>
- Hoffman, J. I. E., & Kaplan, S. (2002). The incidence of congenital heart disease. *Journal of the American College of Cardiology*, *39*(12), 1890–1900. [https://doi.org/10.1016/S0735-1097\(02\)01886-7](https://doi.org/10.1016/S0735-1097(02)01886-7)
- Homsy, J., Zaidi, S., Shen, Y., Ware, J. S., Samocha, K. E., Karczewski, K. J., DePalma, S. R., McKean, D., Wakimoto, H., Gorham, J., Jin, S. C., Deanfield, J., Giardini, A., Porter, G. A., Jr., Kim, R., Bilguvar, K., López-Giráldez, F., Tikhonova, I., Mane, S., ... Chung, W. K. (2015). De novo mutations in congenital heart disease with neurodevelopmental and other birth defects. *Science*, *350*, 1262–1266. <https://doi.org/10.1126/science.aac9396>
- Horev, G., Ellegood, J., Lerch, J. P., Son, Y.-E. E., Muthuswamy, L., Vogel, H., Krieger, A. M., Buja, A., Mark Henkelman, R., Wigler, M., Mills, A. A., & Designated, A. A. M. (2011). Dosage-dependent phenotypes in models of 16p11.2 lesions found in autism/analytic tools; G. *PNAS*, *108*(41), 17076–17081. <https://doi.org/10.1073/pnas.1114021108>
- Hubert, F., Payan, S. M., & Rochais, F. (2018). FGF10 signaling in heart development, homeostasis, disease and repair. *Frontiers in Genetics*, *9*, 1–7. <https://doi.org/10.3389/fgene.2018.00599>
- Human Protein Atlas (n.d.). <https://www.proteinatlas.org/about/licence>
- Janssen, P. M. L., Biesiadecki, B. J., Ziolo, M. T., & Davis, J. P. (2016). The need for speed: Mice, men, and myocardial kinetic reserve. *Circulation Research*, *119*(3), 418–421. <https://doi.org/10.1161/CIRCRESAHA.116.309126>
- Jaramillo, T. C., Speed, H. E., Xuan, Z., Reimers, J. M., Liu, S., & Powell, C. M. (2016). Altered striatal synaptic function and abnormal behaviour in Shank3 Exon4-9 deletion mouse model of autism. *Autism Research*, *9*(3), 350–375. <https://doi.org/10.1002/aur.1529>
- Kaltman, J. R., Di, H., Tian, Z., & Rychik, J. (2005). Impact of congenital heart disease on cerebrovascular blood flow dynamics in the fetus. *Ultrasound in Obstetrics and Gynecology*, *25*(1), 32–36. <https://doi.org/10.1002/uog.1785>
- Karlsson, M., Zhang, C., Méar, L., Zhong, W., Digre, A., Katona, B., Sjöstedt, E., Butler, L., Odeberg, J., Dusart, P., Edfors, F., Oksvold, P., von Feilitzen, K., Zwahlen, M., Arif, M., Altay, O., Li, X., Ozcan, M., Mardinoglu, A., Fagerberg, L., ... Lindskog, C. (2021). A single-cell type transcriptomics map of human tissues. *Science Advances*, *7*(31), 1–10. <https://doi.org/10.1126/sciadv.abh2169>
- Kelm, M., Schäfer, S., Mingers, S., Heydthausen, M., Vogt, M., Motz, W., & Strauer, B. E. (1996). Left ventricular mass is linked

- to cardiac noradrenaline in normotensive and hypertensive patients. *Journal of Hypertension*, 14(11), 1357–1364.
- Kivitie-Kallio, S., Eronen, M., Lipsanen-Nyman, M., Marttinen, E., & Norio, R. (1999). Cohen syndrome: Evaluation of its cardiac, endocrine and radiological features. *Clinical Genetics*, 56, 41–50.
- Kivitie-kallio, S., & Norio, R. (2001). Cohen syndrome: Essential features, natural history, and heterogeneity. *American Journal of Medical Genetics*, 102, 125–135.
- Krishnan, A., Samtani, R., Dhanantwari, P., Lee, E., Yamada, S., Shiota, K., Donofrio, M. T., Leatherbury, L., & Lo, C. W. (2014). A detailed comparison of mouse and human cardiac development. *Pediatric Research*, 76(6), 500–507. <https://doi.org/10.1038/pr.2014.128>
- Kumar, S., Reynolds, K., Ji, Y., Gu, R., Rai, S., & Zhou, C. J. (2019). Impaired neurodevelopmental pathways in autism spectrum disorder: A review of signaling mechanisms and crosstalk. *Journal of Neurodevelopmental Disorders*, 11(10), 1–14.
- Lázaro, M. T., & Golshani, P. (2015). The utility of rodent models of autism spectrum disorders. *Current Opinion in Neurology*, 28(2), 103–109. <https://doi.org/10.1097/WCO.0000000000000183>
- Lee, M.-Y., Won, H.-S., Baek, J. W., Cho, J.-H., Shim, J.-Y., Lee, P.-R., & Kim, A. (2014). Variety of prenatally diagnosed congenital heart disease in 22q11.2 deletion syndrome. *Obstetrics & Gynecology Science*, 57(1), 11. <https://doi.org/10.5468/ogs.2014.57.1.11>
- Lee, Y. K., Hwang, S. K., Lee, S. K., Yang, J. E., Kwak, J. H., Seo, H., Ahn, H., Lee, Y. S., Kim, J., Lim, C. S., Kaang, B. K., Lee, J. H., Lee, J. A., & Lee, K. (2020). Cohen syndrome patient ipsc-derived neurospheres and forebrain-like glutamatergic neurons reveal reduced proliferation of neural progenitor cells and altered expression of synapse genes. *Journal of Clinical Medicine*, 9(6), 1–20. <https://doi.org/10.3390/jcm9061886>
- Li, M., Shin, J., Risgaard, R. D., Parries, M. J., Wang, J., Chasman, D., Liu, S., Roy, S., Bhattacharyya, A., & Zhao, X. (2020). Identification of FMR1-regulated molecular networks in human neurodevelopment. *Genome Research*, 30(3), 361–374. <https://doi.org/10.1101/gr.251405.119>
- Liang, D., Xue, J., Geng, L., Zhou, L., Lv, B., Zeng, Q., Xiong, K., Zhou, H., Xie, D., Zhang, F., Liu, J., Liu, Y., Li, L., Yang, J., Xue, Z., & Chen, Y. H. (2021). Cellular and molecular landscape of mammalian sinoatrial node revealed by single-cell RNA sequencing. *Nature Communications*, 12(1), 287. <https://doi.org/10.1038/s41467-020-20448-x>
- Licht, D. J., Shera, D. M., Clancy, R. R., Wernovsky, G., Montenegro, L. M., Nicolson, S. C., Zimmerman, R. A., Spray, T. L., Gaynor, J. W., & Vossough, A. (2009). Brain maturation is delayed in infants with complex congenital heart defects. *The Journal of Thoracic and Cardiovascular Surgery*, 137(3), 529–537. <https://doi.org/10.1038/jid.2014.371>
- Lim, S., Naisbitt, S., Yoon, J., Hwang, J., Suh, P., Sheng, M., & Kim, E. (1999). Characterization of the shank family of synaptic proteins. *Journal of Biological Chemistry*, 274(41), 29510–29518.
- Limperopoulos, C., Tworetzky, W., McElhinney, D. B., Newburger, J. W., Brown, D. W., Robertson, R. L., Guizard, N., McGrath, E., Geva, J., Annesse, D., Dunbar-Masterson, C., Trainor, B., Laussen, P. C., & du Plessis, A. J. (2010). Brain volume and metabolism in fetuses with congenital heart disease: Evaluation with quantitative magnetic resonance imaging and spectroscopy. *Circulation*, 121(1), 26–33. <https://doi.org/10.1161/CIRCULATIONAHA.109.865568>
- Loomes, R., Hull, L., & Mandy, W. P. L. (2017). What is the male-to-female ratio in autism spectrum disorder? A systematic review and meta-analysis. *Journal of the American Academy of Child and Adolescent Psychiatry*, 56(6), 466–474. <https://doi.org/10.1016/j.jaac.2017.03.013>
- Makowski, D., Ben-Shachar, M., & Lüdtke, D. (2019). bayestestR: Describing effects and their uncertainty, existence and significance within the Bayesian framework. *Journal of Open Source Software*, 4(40), 1541. <https://doi.org/10.21105/joss.01541>
- Makowski, D., Ben-Shachar, M. S., Chen, S. H. A., & Lüdtke, D. (2019). Indices of effect existence and significance in the Bayesian framework. *Frontiers in Psychology*, 10, 1–14. <https://doi.org/10.3389/fpsyg.2019.02767>
- Man, W., Gu, J., Wang, B., Zhang, M., Hu, J., & Lin, J. (2020). SHANK3 co-ordinately regulates autophagy and apoptosis in myocardial infarction. *Frontiers in Physiology*, 11(1082), 1–10. <https://doi.org/10.3389/fphys.2020.01082>
- Marino, B. S., Lipkin, P. H., Newburger, J. W., Peacock, G., Gerdes, M., Gaynor, J. W., Mussatto, K. A., Uzark, K., Goldberg, C. S., Johnson, W. H., Li, J., Smith, S. E., Bellinger, D. C., & Mahle, W. T. (2012). Neurodevelopmental outcomes in children with congenital heart disease: Evaluation and management a scientific statement from the American heart association. *Circulation*, 126(9), 1143–1172. <https://doi.org/10.1161/CIR.0b013e318265ee8a>
- Marques Ribeiro, E., Brusius-facchin, A. C., Leistner-segal, S., Antônio, C., & Vanessa, I. (2014). Cardiac disease as the presenting feature of mucopolysaccharidosis type IIIA: A case report. *Molecular Genetics and Metabolism Reports*, 1, 422–424. <https://doi.org/10.1016/j.ymgmr.2014.09.003>
- Meisner, J. K., & Martin, D. M. (2020). Congenital heart defects in CHARGE: The molecular role of CHD7 and effects on cardiac phenotype and clinical outcomes. *American Journal of Medical Genetics, Part C: Seminars in Medical Genetics*, 184(1), 81–89. <https://doi.org/10.1002/ajmg.c.31761>
- Metcalfe, K. (2018). Cardiac problems in genetic syndromes. *Paediatrics and Child Health (United Kingdom)*, 28(12), 574–578. <https://doi.org/10.1016/j.paed.2018.10.005>
- Milani-Nejad, N., & Janssen, P. M. L. (2014). Small and large animal models in cardiac contraction research: Advantages and disadvantages. *Pharmacology and Therapeutics*, 141(3), 235–249. <https://doi.org/10.1016/j.pharmthera.2013.10.007>
- Miller, S. P., McQuillen, P. S., Hamrick, S., Xu, D., Glidden, D., Charlton, N., Karl, T., Azakie, A., Ferriero, D. M., Barkovich, A. J., & Vigneron, D. B. (2007). Abnormal brain development in newborns with congenital heart disease. *New England Journal of Medicine*, 357(19), 1928–1938. <https://doi.org/10.1056/NEJMoa067393>
- Miot, S., Akbaraly, T., Michelon, C., Couderc, S., Crepiat, S., Loubersac, J., Picot, M. C., Pernon, É., Gonnier, V., Jeandel, C., Blain, H., & Baghdadli, A. (2019). Comorbidity burden in adults with autism Spectrum disorders and intellectual disabilities—A report from the EFAAR (frailty assessment in ageing adults with autism Spectrum and intellectual disabilities) study. *Frontiers in Psychiatry*, 10(617), 1–13. <https://doi.org/10.3389/fpsy.2019.00617>
- Morales-Demori, R. (2017). Congenital heart disease and cardiac procedural outcomes in patients with trisomy 21 and turner syndrome. *Congenital Heart Disease*, 12(6), 820–827. <https://doi.org/10.1111/chd.12521>
- Moss, J., & Howlin, P. (2009). Autism spectrum disorders in genetic syndromes: Implications for diagnosis, intervention and understanding the wider autism spectrum disorder population. *Journal of Intellectual Disability Research*, 53(10), 852–873. <https://doi.org/10.1111/j.1365-2788.2009.01197.x>
- Napolitano, C., Timothy, K. W., Bloise, R., & Priori, S. G. (2006). CACNA1C-related disorders. In M. P. Adam, H. H. Ardinger & R. A. Pagon (Eds.), *GeneReviews*. Seattle (WA): University of Washington, Seattle. <https://www.ncbi.nlm.nih.gov/books/NBK1403/>
- Nazeen, S., Palmer, N. P., Berger, B., & Kohane, I. S. (2016). Integrative analysis of genetic data sets reveals a shared innate immune component in autism spectrum disorder and its co-morbidities. *Genome Biology*, 17(1), 228. <https://doi.org/10.1186/s13059-016-1084-z>

- Nijmeijer, S. C. M., de Bruin-Bon, R. H. A. C. M., Wijburg, F. A., & Kuipers, I. M. (2019). Cardiac disease in mucopolysaccharidosis type III. *Journal of Inherited Metabolic Disease*, *42*, 276–285. <https://doi.org/10.1002/jimd.12015>
- Nishiyama, M., Oshikawa, K., Tsukada, Y., Nakagawa, T., & Nakayama, K. I. (2011). CHD8 suppresses p53-mediated apoptosis through histone H1 recruitment during early embryogenesis. *Nature Cell Biology*, *11*(2), 172–182. <https://doi.org/10.1038/ncb1831>
- Noujaim, S. F., Lucca, E., Muñoz, V., Persaud, D., Berenfeld, O., Meijler, F. L., & Jalife, J. (2004). From mouse to whale: A universal scaling relation for the PR interval of the electrocardiogram of mammals. *Circulation*, *110*(18), 2802–2808. <https://doi.org/10.1161/01.CIR.0000146785.15995.67>
- Ornoy, A., Liza, W. F., & Ergaz, Z. (2016). Genetic syndromes, maternal diseases and antenatal factors associated with autism spectrum disorders (ASD). *Frontiers in Neuroscience*, *10*, 1–21. <https://doi.org/10.3389/fnins.2016.00316>
- Ortinau, C. M., Mangin-Heimos, K., Moen, J., Alexopoulos, D., Inder, T. E., Gholipour, A., Shimony, J. S., Eghtesady, P., Schlaggar, B. L., & Smyser, C. D. (2018). Prenatal to postnatal trajectory of brain growth in complex congenital heart disease. *NeuroImage: Clinical*, *20*, 913–922. <https://doi.org/10.1016/j.nicl.2018.09.029>
- Pagon, R. A., Graham, J. M., Zonana, J., & Yong, S. L. (1981). Coloboma, congenital heart disease, and choanal atresia with multiple anomalies: CHARGE association. *The Journal of Pediatrics*, *99*(2), 223–227. [https://doi.org/10.1016/S0022-3476\(81\)80454-4](https://doi.org/10.1016/S0022-3476(81)80454-4)
- Patel, M. B., Stewart, J. M., Loud, A., Anversa, P., Wang, J., Fiegel, L., & Hintze, T. H. (1991). Altered function and structure of the heart in dogs with chronic elevation in plasma norepinephrine. *Circulation*, *84*(5), 2091–2100. <https://doi.org/10.1161/01.CIR.84.5.2091>
- Patel, N., & Makaryus, A. N. (2020). Physiology. Cardiac index. *StatPearls [Internet]* (Vol. 20894). Treasure Island (FL): StatPearls Publishing. <http://www.ncbi.nlm.nih.gov/pubmed/30969727>
- Pet, S., Kreissl, M. C., Wu, H., Stout, D. B., Ladno, W., Schindler, T. H., Zhang, X., Prior, J. O., Prins, M. L., Chatziioannou, A. F., Huang, S., & Schelbert, H. R. (2006). Non-invasive measurement of cardiovascular function in mice with high-temporal-resolution. *Journal of Nuclear Medicine*, *47*(6), 974–980.
- Phelan, K., & McDermid, H. E. (2012). The 22q13.3 deletion syndrome (Phelan-McDermid syndrome). *Molecular Syndromology*, *2*(3–5), 186–201. <https://doi.org/10.1159/000334260>
- Pierpont, M. E., Brueckner, M., Chung, W. K., Garg, V., Lacro, R., McGuire, A. L., Mital, S., Priest, J. R., Pu, W. T., Roberts, A., Ware, S. M., Gelb, B. D., & Russell, M. W. (2018). Genetic basis for congenital heart disease: Revisited: A scientific statement from the American Heart Association. *Circulation*, *138*, e653–e711. <https://doi.org/10.1161/CIR.0000000000000606>
- R Core Team. (2019). *R: A language and environment for statistical computing* (p. 3.6.1). R Foundation for Statistical Computing <https://www.r-project.org/>
- Regitz-Zagrosek, V., & Kararigas, G. (2017). Mechanistic pathways of sex differences in cardiovascular disease. *Physiological Reviews*, *97*(1), 1–37. <https://doi.org/10.1152/physrev.00021.2015>
- Rodrigues, J. M., Fernandes, H. D., Caruthers, C., Braddock, S. R., & Knutsen, A. P. (2018). Cohen syndrome: Review of the literature. *Cureus*, *10*(9), 1–8. <https://doi.org/10.7759/cureus.3330>
- Rosenthal, S. B., Willsey, H. R., Xu, Y., Mei, Y., Dea, J., Wang, S., Curtis, C., Sempou, E., Khokha, M. K., Chi, N. C., Willsey, A. J., Fisch, K. M., & Ideker, T. (2021). A convergent molecular network underlying autism and congenital heart disease. *Cell Systems*, *1–14*, 1094–1107.e6. <https://doi.org/10.1016/j.cels.2021.07.009>
- RStudio. (2019). *RStudio: Integrated development for R*. RStudio <http://www.rstudio.com/>
- Rumsey, R. K., Rudser, K., Delaney, K., Potegal, M., Whitley, C. B., & Shapiro, E. (2014). Acquired autistic behaviors in children with mucopolysaccharidosis type IIIA. *Journal of Pediatrics*, *164*(5), 1147–1151.e1. <https://doi.org/10.1016/j.jpeds.2014.01.007>
- Sadowski, S. L. (2009). Congenital cardiac disease in the newborn infant: Past, present, and future. *Critical Care Nursing Clinics of North America*, *21*(1), 37–48. <https://doi.org/10.1016/j.ccell.2008.10.001>
- Schlaich, M. P., Kaye, D. M., Lambert, E., Somerville, M., Socratous, F., & Esler, M. D. (2003). Relation between cardiac sympathetic activity and hypertensive left ventricular hypertrophy. *Circulation*, *108*(5), 560–565. <https://doi.org/10.1161/01.CIR.0000081775.72651.B6>
- Shanks, M. O., Lund, L. M., Manni, S., Russell, M., Mauban, J. R. H., & Bond, M. (2012). Chromodomain helicase binding protein 8 (Chd8) is a novel A-kinase anchoring protein expressed during rat cardiac development. *PLoS One*, *7*(10), e46316. <https://doi.org/10.1371/journal.pone.0046316>
- Sheinkopf, S. J., Levine, T. P., McCormick, C. E. B., Puggioni, G., Conrath, E., Lagasse, L. L., & Lester, B. M. (2019). Developmental trajectories of autonomic functioning in autism from birth to early childhood. *Biological Psychology*, *142*, 13–18. <https://doi.org/10.1016/j.biopsycho.2019.01.003>
- Sigmon, E. R., Kelleman, M., Susi, A., Nylund, C. M., & Oster, M. E. (2019). Congenital heart disease and autism: A case-control study. *Pediatrics*, *144*(5), 2018–4114. <https://doi.org/10.1542/peds.2018-4114>
- Silvani, A., Calandra-buonaura, G., Dampney, R. A. L., Cortelli, P., & Cortelli, P. (2016). Brain–Heart interactions: Physiology and clinical implications subject areas: Author for correspondence. *The Royal Society Publishing*, *374*, 1–22.
- Snider, P., & Conway, S. J. (2011). Probing human cardiovascular congenital disease using transgenic mouse models. *Progress in Molecular Biology and Translational Science*, *100*, 83–110. <https://doi.org/10.1016/B978-0-12-384878-9.00003-0>
- Stan Development Team. (2017). Stan Modeling Language Users Guide and Reference Manual, 2.29. <https://mc-stan.org>
- Storey, J. D. (2003). The positive false discovery rate: A Bayesian interpretation and the q-value. *Annals of Statistics*, *31*(6), 2013–2035. <https://doi.org/10.1214/aos/1074290335>
- Sugathan, A., Biagioli, M., Golzio, C., Erdin, S., Blumenthal, I., Manavalan, P., Ragavendran, A., Brand, H., Lucente, D., Miles, J., Sheridan, S. D., Stortchevoi, A., Kellis, M., Haggarty, S. J., Katsanis, N., Gusella, J. F., & Talkowski, M. E. (2014). CHD8 regulates neurodevelopmental pathways associated with autism spectrum disorder in neural progenitors. *Proceedings of the National Academy of Sciences of the United States of America*, *111*(42), E4468–E4477. <https://doi.org/10.1073/pnas.1405266111>
- Sun, H., & Wang, Y. (2016). Branched chain amino acid metabolic reprogramming in heart failure. *Biochimica et Biophysica Acta - Molecular Basis of Disease*, *1862*(12), 2270–2275. <https://doi.org/10.1016/j.bbadis.2016.09.009>
- Sun, L., Macgowan, C. K., Sled, J. G., Yoo, S. J., Manlihot, C., Porayette, P., Grosse-Wortmann, L., Jaeggi, E., McCrindle, B. W., Kingdom, J., Hickey, E., Miller, S., & Seed, M. (2015). Reduced fetal cerebral oxygen consumption is associated with smaller brain size in fetuses with congenital heart disease. *Circulation*, *131*(15), 1313–1323. <https://doi.org/10.1161/CIRCULATIONAHA.114.013051>
- Tassanakijpanich, N., Cohen, J., Cohen, R., Srivatsa, U. N., & Hagerman, R. J. (2020). Cardiovascular problems in the Fragile X Premutation. *Frontiers in Genetics*, *11*, 1–8. <https://doi.org/10.3389/fgene.2020.586910>

- The Dutch-Belgian Fragile X Consortium, Bakker, C. E., Verheij, C., Willemsen, R., van der Helm, R., Oerlemans, F., Vermey, M., Bygrave, A., Hoogeveen, A. T., Oostra, B. A., Reyniers, E., de Boule, K., D'Hooge, R., Cras, P., van Velzen, D., Nagels, G., Martin, J. J., de Deyn, P. P., Darby, J. K., & Willems, P. J. (1994). Fmr1 knockout mice: A model to study fragile X mental retardation. *Cell*, *78*(1), 23–33. [https://doi.org/10.1016/0092-8674\(94\)90569-X](https://doi.org/10.1016/0092-8674(94)90569-X)
- Timme, N., Alford, W., Flecker, B., Beggs, J. M., Timme, N., Alford, W., Flecker, B., & Beggs, J. M. (2014). Synergy, redundancy, and multivariate information measures: An experimentalist's perspective. *Journal of Computational Neuroscience*, *36*, 119–140. <https://doi.org/10.1007/s10827-013-0458-4>
- Tsao, P. C., Lee, Y. S., Jeng, M. J., Hsu, J. W., Huang, K. L., Tsai, S. J., Chen, M. H., Soong, W. J., & Kou, Y. R. (2017). Additive effect of congenital heart disease and early developmental disorders on attention-deficit/hyperactivity disorder and autism spectrum disorder: A nationwide population-based longitudinal study. *European Child and Adolescent Psychiatry*, *26*(11), 1351–1359. <https://doi.org/10.1007/s00787-017-0989-8>
- Tyler, C. V., Schramm, S. C., Karafa, M., Tang, A. S., & Jain, A. K. (2011). Chronic disease risks in young adults with autism spectrum disorder: Forewarned is forearmed. *American Journal on Intellectual and Developmental Disabilities*, *116*(5), 371–380. <https://doi.org/10.1352/1944-7558-116.5.371>
- Vasileiou, G., Ekici, A. B., Uebe, S., Zweier, C., Hoyer, J., Engels, H., Behrens, J., Reis, A., & Hadjihannas, M. (2015). Chromatin-remodeling-factor ARID1B represses Wnt/ β -catenin signaling. *American Journal of Human Genetics*, *97*(3), 445–456. <https://doi.org/10.1016/j.ajhg.2015.08.002>
- Vehtari, A., Gabry, J., Magnusson, M., Yao, Y., Bürkner, P., Paananen, T., & Gelman, A. (2020). loo: Efficient leave-one-out cross-validation and WAIC for Bayesian models.
- Vehtari, A., Gelman, A., & Gabry, J. (2017). Practical Bayesian model evaluation using leave-one-out cross-validation and WAIC. *Journal of Statistical Computation*, *27*(5), 1413–1432. <https://arxiv.org/pdf/1507.04544.pdf>
- Vorstman, J. A. S., Morcus, M. E. J., Duijff, S. N., Klaassen, P. W. J., Heineman-de Boer, J. A., Beemer, F. A., Swaab, H., Kahn, R. S., van Engeland, H. (2006). The 22q11.2 Deletion in Children. *Journal of the American Academy of Child & Adolescent Psychiatry*, *45*(9), 1104–1113. <https://doi.org/10.1097/01.chi.0000228131.56956.c1>
- Wang, Y. (2007). Mitogen-activated protein kinases in heart development and diseases. *Circulation*, *116*(12), 1413–1423. <https://doi.org/10.1161/CIRCULATIONAHA.106.679589>
- Webb, T. R., Erdmann, J., Stirrups, K. E., Stitzel, N. O., Masca, N. G. D., Jansen, H., Kanoni, S., Nelson, C. P., Ferrario, P. G., König, I. R., Eicher, J. D., Johnson, A. D., Hamby, S. E., Betsholtz, C., Ruusalepp, A., Franzén, O., Schadt, E. E., Björkegren, J. L. M., Weeke, P. E., ... Kathiresan, S. (2017). Systematic evaluation of pleiotropy identifies 6 further loci associated with coronary artery disease. *Journal of the American College of Cardiology*, *69*(7), 823–836. <https://doi.org/10.1016/j.jacc.2016.11.056>
- Wen, Y., & Li, B. (2015). Morphology of mouse sinoatrial node and its expression of NF-160 and HCN4. *International Journal of Clinical and Experimental Medicine*, *8*(8), 13383–13387.
- Wessels, A., & Sedmera, D. (2004). Developmental anatomy of the heart: A tale of mice and man. *Physiological Genomics*, *15*, 165–176. <https://doi.org/10.1152/physiolgenomics.00033.2003>
- Wiese, C., Grieskamp, T., Airik, R., Mommersteeg, M. T. M., Gardiwal, A., de Gier-De Vries, C., Schuster-Gossler, K., Moorman, A. F. M., Kispert, A., & Christoffels, V. M. (2009). Formation of the sinus node head and differentiation of sinus node myocardium are independently regulated by Tbx18 and Tbx3. *Circulation Research*, *104*(3), 388–397. <https://doi.org/10.1161/CIRCRESAHA.108.187062>
- Wijburg, F. A., W grzyn, G., Burton, B. K., & Tylki-Szymańska, A. (2013). Mucopolysaccharidosis type III (Sanfilippo syndrome) and misdiagnosis of idiopathic developmental delay, attention deficit/hyperactivity disorder or autism spectrum disorder. *Acta Paediatrica, International Journal of Paediatrics*, *102*(5), 462–470. <https://doi.org/10.1111/apa.12169>
- Wu, W., He, J., & Shao, X. (2020). Incidence and mortality trend of congenital heart disease at the global, regional, and national level, 1990–2017. *Medicine (United States)*, *99*(23), e20593. <https://doi.org/10.1097/MD.00000000000020593>
- Xie, H., Hong, N., Zhang, E., Li, F., Sun, K., & Yu, Y. (2019). Identification of rare copy number variants associated with pulmonary atresia with ventricular septal defect. *Frontiers in Genetics*, *10*, 1–11. <https://doi.org/10.3389/fgene.2019.00015>
- Xu, M., Yao, J., Shi, Y., Yi, H., Zhao, W., Lin, X., & Yang, Z. (2021). The SRCAP chromatin remodeling complex promotes oxidative metabolism during prenatal heart development. *Development (Cambridge)*, *148*(8), 1–12. <https://doi.org/10.1242/dev.199026>
- Zerbi, V., Pagani, M., Markicevic, M., Matteoli, M., Pozzi, D., Fagiolini, M., Bozzi, Y., Galbusera, A., Scattoni, M. L., Provenzano, G., Banerjee, A., Helmchen, F., Basson, M. A., Ellegood, J., Lerch, J. P., Rudin, M., Gozzi, A., & Wenderoth, N. (2021). Brain mapping across 16 autism mouse models reveals a spectrum of functional connectivity subtypes. *Molecular Psychiatry*, *26*, 7610–7620. <https://doi.org/10.1038/s41380-021-01245-4>
- Zhang, P., Lu, H., Peixoto, R. T., Pines, M. K., Ge, Y., Oku, S., Siddiqui, T. J., Xie, Y., Wu, W., Archer-Hartmann, S., Yoshida, K., Tanaka, K. F., Aricescu, A. R., Azadi, P., Gordon, M. D., Sabatini, B. L., Wong, R. O. L., & Craig, A. M. (2018). Heparan sulfate organizes neuronal synapses through Neurexin partnerships. *Cell*, *174*(6), 1450–1464.e23. <https://doi.org/10.1016/j.cell.2018.07.002>
- Zhou, Y.-Q., Foster, F. S., Nieman, B. J., Davidson, L., Chen, X. J., & Henkelman, R. M. (2004). Comprehensive transthoracic cardiac imaging in mice using ultrasound biomicroscopy with anatomical confirmation by magnetic resonance imaging. *Physiological Genomics*, *18*, 232–244.
- Zoghbi, W. A., Habib, G. B., & Quinones, M. A. (1990). Doppler assessment of right ventricular filling in a Normal population. *Circulation*, *82*(4), 1316–1324.

SUPPORTING INFORMATION

Additional supporting information may be found in the online version of the article at the publisher's website.

How to cite this article: Assimopoulos, S., Hammill, C., Fernandes, D. J., Spencer Noakes, T. L., Zhou, Y.-Q., Nutter, L. M. J., Ellegood, J., Anagnostou, E., Sled, J. G., & Lerch, J. P. (2022). Genetic mouse models of autism spectrum disorder present subtle heterogeneous cardiac abnormalities. *Autism Research*, *15*(7), 1189–1208. <https://doi.org/10.1002/aur.2728>